Naval Research Laboratory

Stennis Space Center, MS 39529-5004

NRL/MR/7330--13-9447

Anode Material Testing for Marine Sediment Microbial Fuel Cells

ANDREW JOHN QUAID

Ocean Sciences Branch
Oceanography Division

September 26, 2013

REPORT DOCUMENTATION PAGE

Form Approved
OMB No. 0704-0188

1. REPORT DATE *(DD-MM-YYYY)*	2. REPORT TYPE	3. DATES COVERED *(From - To)*
26-09-2013	Memorandum Report	

4. TITLE AND SUBTITLE

Anode Material Testing for Marine Sediment Microbial Fuel Cells

5a. CONTRACT NUMBER

5b. GRANT NUMBER

5c. PROGRAM ELEMENT NUMBER
0602435N

6. AUTHOR(S)

Andrew John Quaid

5d. PROJECT NUMBER

5e. TASK NUMBER

5f. WORK UNIT NUMBER
73-6358-B2-5

7. PERFORMING ORGANIZATION NAME(S) AND ADDRESS(ES)

Naval Research Laboratory
Oceanography Division
Stennis Space Center, MS 39529-5004

8. PERFORMING ORGANIZATION REPORT NUMBER

NRL/MR/7330--13-9447

9. SPONSORING / MONITORING AGENCY NAME(S) AND ADDRESS(ES)

Office of Naval Research
One Liberty Center
875 North Randolph Street, Suite 1425
Arlington, VA 22203-1995

10. SPONSOR / MONITOR'S ACRONYM(S)

ONR

11. SPONSOR / MONITOR'S REPORT NUMBER(S)

12. DISTRIBUTION / AVAILABILITY STATEMENT

Approved for public release; distribution is unlimited.

13. SUPPLEMENTARY NOTES

14. ABSTRACT

An increase in scientific research of microbial fuel cell technology is usually based on increasing the efficiency of the fuel cell by modifying the components or via investigations based on the microbiology that catalyzes the electrochemistry of the system. The increase of efficiency in sediment microbial fuel cells may lead to increased deployment times and reduction of battery requirements for oceanographic sensor systems. In a two-part study, anode material types with different surface area and porosity properties were compared and exoelectrogenic and background bacterial populations were detected and relatively quantified using real-time PCR techniques. The different types of anode material were tested under controlled conditions in a tank of marine sediment, keeping temperature, salinity, oxygen content, and the flow of interstitial water across the anode material as stable as possible. The relative quantification of biofilm was investigated using the relative real-time polymerase chain reaction method and aragose gel electrophoresis.

15. SUBJECT TERMS

Anode material
Microbial fuel cell
Relative PCR
Marine sediment

16. SECURITY CLASSIFICATION OF:			17. LIMITATION OF ABSTRACT	18. NUMBER OF PAGES	19a. NAME OF RESPONSIBLE PERSON
a. REPORT	b. ABSTRACT	c. THIS PAGE			Andrew Quaid
Unclassified Unlimited	Unclassified Unlimited	Unclassified Unlimited	Unclassified Unlimited	86	19b. TELEPHONE NUMBER *(include area code)* (228) 688-5454

TABLE OF CONTENTS

LIST OF TABLES iv

LIST OF ILLUSTRATIONS v

ABSTRACT vii

CHAPTER

I. INTRODUCTION 1

Abstract
Background
Objectives
Significance of the Study
Hypothesis

II. METHODS AND MATERIALS 7

Sediment Microbial Fuel Cell
Test Tank
Scribner Associates 871 Electrical Load Cell
Microbial DNA Sampling and Analysis

III. RESULTS 20

Sediment Microbial Fuel Cell Power Production
Approximate Surface Area and Porosity of Graphite Foam Billets
Electrical Power Production of Anode Configurations
Detection and Relative Enrichment Study of *Geobacteraceae* and Bacterial PCR Targets

IV. DISCUSSION 56

Sediment Microbial Fuel Cell Power Production
Surface Area and Volume of Anode Material
Electrical Power Produced by Anode Type
Detection and Relative Enrichment of *Geobacteracea* 16S rRNA Primer Targets

V. CONCLUSION 66

APPENDIXES 68

REFERENCES 75

LIST OF TABLES

Table

1. Summary of Graphite Anode Material Volume and Approximate Surface Area....9

2. Summary of Electrical Testing Procedure and Durations of Anode Types....15

3. Summary of Approximate Surface Area and Porosity of Anode Material from Volumetric Study....22

4. Summary of SMFC Power Production Tests, including Dates, Logging interval, Temperature, Salinity....24

LIST OF ILLUSTRATIONS

Figure

1. Sediment Microbial Fuel Cell Illustration 2
2. Image of Graphite Foam Billets and Solid Graphite Plate Anode....8
3. Image of Graphite Foam Billet in Pump Chamber 10
4. Graphical Representation of Plate and Foam Plate Configuration 11
5. Graphite Fiber Bottle Brush Cathode 12
6. Electrical Diagram of Electronic Load System 14
7. Graphical representation of DNA Sampling of Graphite Foam Anodes 16
8. Data Graph of Temperature and Salinity of Test Tank....21
9. Data Graphs of Electrical Tests of Solid Graphite Plate Anode....27
10. Data Graphs of Electrical Tests of 45 PPI Graphite Foam Anode 29
11. Data Graphs of Electrical Tests of Kfoam Graphite Foam Anode 31
12. Data Graphs of Electrical Tests of 80 PPI Graphite Foam Anode 33
13. Data Graphs of Electrical Tests of 45 PPI Foam Plate Configuration....35
14. Data Graph of Power Density Curves for Foam and Plate Anodes....37
15. Data Graphs of Downscaling of Solid Graphite Plate 38
16. Data Graphs of Relative PCR Comparison of All Sediment Samples....42
17. Data Graphs of Relative PCR Comparison of Solid Graphite Plate Anode 43
18. Data Graphs of Relative PCR comparison of 80 PPI Graphite Foam Anode....45
19. Data Graphs of Relative PCR Comparison of 45 PPI Graphite Foam Anode....46
20. Data Graphs of Relative PCR Comparison of Kfoam Anode....48
21. Data Graphs of Relative PCR Comparison of 45 PPI Foam Plate Anode....49
22. Image of Aragose Gel Electrophoresis of Selected Anode Samples 52

23. Data Graphs of Selected C_T Values of 45 PPI Anode Samples 53

24. Data Graph of Melt Curves for 45 PPI Anode Samples 55

ABSTRACT

Research on the power production of the microbial fuel cell has increased in the past decade. The sediment microbial fuel cell is a type of fuel cell that uses the environment of submerged sediments to provide a natural voltage difference. The fuel cell is comprised of an anode buried in the sediment and a cathode that is held in the overlying water column. The process of electron transfer to the anode is catalyzed by anaerobic bacteria in the sediment. The anaerobic bacteria have that are able to catalyze the electron transfer have been termed exoelectrogenic. The increase in scientific research of microbial fuel cell technology is based on increasing the efficiency of the fuel cell by modifying the components of the fuel cell, or studying the microbiology which catalyzes the electrochemistry of the system. The increase of efficiency in sediment microbial fuel cells may lead to the powering of oceanographic senor systems, for increase deployment times, and reduce the quantity of batteries needed for these systems.

This study has two components, firstly, the comparison of power production from anode material with differing surface area and porosity properties, and secondly, to detect and relatively quantify the exoelectrogenic bacteria that may form biofilms on the anode material. A test tank was used to compare the different types of anode material under controlled conditions, keeping the temperature, salinity, oxygen content, and the flow of interstitial water across the anode material, as stable as possible. The second part of the study was completed by using relative real-time polymerase chain reaction method and aragose gel electrophoresis.

CHAPTER I

INTRODUCTION

Background

Studies of microbial fuel cell (MFC) electrical power generation were first published in 1962 (1). Over the past decade there has been a dramatic increase in both the number and types of studies into the MFC. The increase in MFC studies have focused on a diversity of applications, such as wastewater treatment, powering environmental sensors, bioremediation, and hydrogen production (2, 3, 4, 5, 6). A subcategory of the MFC is the sediment microbial fuel cell (SMFC), for which the aquatic sediments are used as a component in the fuel cell (2, 7, 8). The SMFC is usually configured by placing a graphite anode in the anoxic environment found in many types of marine sediment, and connected by means of an external electrical circuit to a graphite cathode in the overlying oxygenated water (Figure 1, 9). The electrochemical process of the SMFC consists of the anode collecting respired electrons from microbial oxidation of sedimentary organic matter, resulting in electrons flowing through the external circuit to the cathode where reduction of oxygen occurs (10, 11, 12). The charge and mass balances are maintained by protons, which are generated at the anode, migrate to the water column and consumed at the cathode (2). Studies show that members of the *Geobacteraceae* family of bacteria, *Shewanella* spp. (13, 14, 15, 16), *Rhodoferax ferrireducens* (17), *Aeromonas hydrophila* (18), *Pseudomonas aeruginosa* (19), *Clostridium butyricum* (20), and *Enterococcus gallinarum* (15), preferentially colonize, or have been inoculated to the anodes and catalyze the anode reaction of multiple types of MFC systems (21). The fuel cells deployed in the natural environment have a mixed-culture biofilm, which has been shown to produce more power than the pure cultured

Manuscript approved October 29, 2012.

counterparts (16, 22). The *Geobacteraceae* family has been shown to be a majority of the population of the biofilm that forms on the anode of SMFCs deployed in natural marine and freshwater sediments (11, 22, 16).

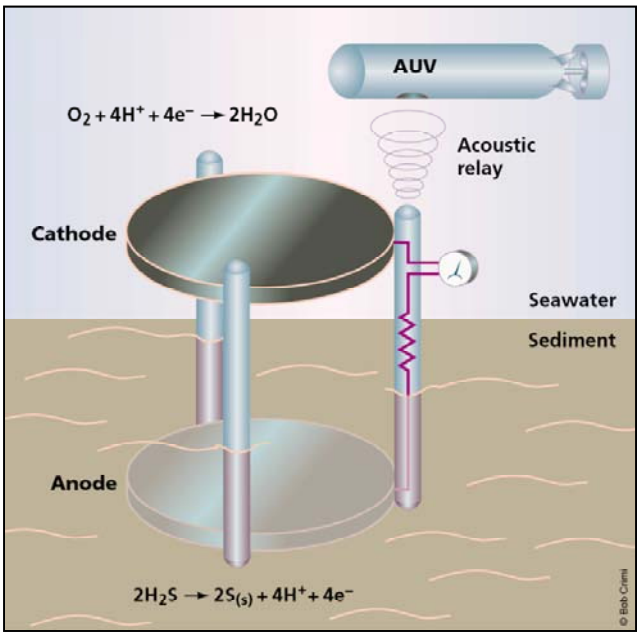

Figure 1. Sediment Microbial Fuel Cell: This image shows the potential use of sediment microbial fuel cells. This depiction shows an acoustic sensor (represented by generic dial) transmitting or receiving data from an autonomous underwater vehicle (AUV). The half cell reaction is depicted here as the microbial oxidations of H2S producing electrons in the sediment, and in the water column, oxygen is being reduced to water. (22)

In most of the above studies, the identifications of the microorganisms that grow on the anodic surfaces of the microbial fuel cells were found through polymerase chain reaction techniques (13, 14, 15, 16, 17, 23, 19, 20, 15). With conventional PCR techniques, an extracted DNA sample is amplified multiple times, and this amplification is detected with the real-time PCR system, and the use of an agarose gel electrophoresis technique (24, 8, 25). This allows the visual interpretation of the size and concentration of the DNA as compared to a mass ladder (26).

The description of the cell voltage of the MFC is usually a linear function of current, with a simplified form of

$$E_{cell} = OCV - I \times R_{int}$$

where E_{cell} is the voltage for the entire cell. The OCV is the open circuit voltage, where no connection between anode and cathode exists, and thus no current flows (7). The variable I is current and R_{int} is the internal resistance (7). As of 2007, the highest OCV reported in a SMFC was 0.86 volts, which is lower than the theoretical OCV of 1.1 volts (20). The theoretical OCV is determined from the electromotive force (EMF) equation of the cell, which is determined from the Gibbs free energy of the separate reactions occurring at the anode and cathode (7). The Gibbs free energy is calculated from the half reactions of acetate oxidization at the anode, and oxygen reduction at the cathode (7). The cell EMF has the form of

$$E_{emf} = E_{cat} - E_{an}$$

where E_{emf} is the overall theoretical electromotive force, E_{cat} is the electromotive force of the half-cell reaction of the cathode, and E_{an} is the electromotive force of the half-cell reaction of the anode (7). The difference in the theoretical EMF of the cell, and the measured OCV is defined as the overvoltage (7, 8).

The limiting factors are described in four general categories of ohmic losses, activation losses, bacterial metabolic losses, and mass transport or concentration losses (7, 8). The ohmic losses of the cell are from the resistance of the electrons to flow from anode to cathode, and the resistance of the protons to migrate from the anode to cathode, and the conductivity of the electrolytes (7, 8). Activation losses are those that occur during the transfer of the electron from or to a compound reacting at the electrode surface, such as a mediator compound (7, 8). The Bacterial Metabolic ohmic loss is found between the

balance between the difference of the redox potential of the substrate and the potential of the anode (7, 8). The higher the difference in the two potentials the more energy is gained by the bacteria when the electron is transported from substrate to anode, but if the electrode is kept at too low of a potential, the electron transport will be inhibited (7, 8). Concentration losses are developed from a slow rate of mass transport occurring at the electrode (7, 8). At the anode this will can be either a slow supply of reduced chemical species (the food), or a buildup of oxidized chemical species (by products), which can in turn raise the potential of the anode, decreasing the energy produced (7, 8).

The focus of this study is the anode materials used to form a sediment microbial fuel cell (SMFC). Documenting the electrical production and the enrichment of exoelectrogenic microbes that occur with different types of anode materials, will increase the knowledge of the SMFCs. The results of this study will allow for a more informed choice of anode material for SMFC which can then be used for the energizing of oceanographic sensors. The results may also be used for the comparison of SMFC used in the marine environment.

Objectives

This experiment is designed to test the variables of surface area and volumes of anode material (e.g. minimize activation losses), and to examine the extent of the bacterial communities which colonize the exterior and interior of the different configurations of SMFC anodes. The surface area for bacterial colonization will be tested by using 3 types of graphite foam billets and a solid graphite plate. Each of the foam billets have different porosities which may allow for more surface area to be colonized by exoelectrogen communities, affecting the activation losses. Also, the different porosities may affect the concentration losses, by allowing more flushing of the

foam. In an attempt to keep the rate of supply of reduced organic material (food) constant in the anode chamber, a volume of interstitial water will be pumped through the foam by using a peristaltic pump. A fourth configuration will take the same volume of a single foam billet, but sliced into three sections with a small gap between each layer of foam. The foam with the best electrical performance will be used for this "foam-plate" configuration, which may allow for more mass transport. The foam billets will also be tested for scalability by incrementally increasing and decreasing the volume of anode during the experiment. Relative C_T comparison will be used to identify anode samples that show enrichment of exoelctrogenic microbes on the anodes. The RT-PCR will enable the detection of enrichment of microbes that may form a biofilm in the interior matrix of the graphite. Gel electrophoresis will be used to verify the PCR results by verifying the base-pair size of the amplicon to those sizes reported by the literature. An estimation of the amplified concentration of the targeted DNA can be made during the gel electrophoresis process.

Significance of Study

Currently, marine SMFC systems have been able to supply electrical energy to low-wattage oceanographic sensors (11). These SMFC systems embed solid graphite plates into the sediment. Increasing the electrical productivity of the SMFC will fulfill the power requirements, or allow for extended deployment times of oceanographic sensor systems. Increasing the electrical generation of SMFC systems may provide a sustainable power source to sensors systems deployed at one of the most remote locations in the world, the bottom of the ocean. This system will likely have a near zero impact on the marine environment, since the anode and cathode material is non-reactive carbon graphite. The development of this technology will impact remote monitoring stations for

marine biology (e.g., migration tracking), oceanographic geological processes (e.g., tsunami warning systems), and national-defense technology (e.g., underwater defense monitoring systems), bioremediation, and may also increase the production of energy from wastewater systems while reducing nutrient loads (2, 3). The success of the SMFC alternative energy system will likely reduce the cost and waste associated with using alkaline and or lithium batteries, and the cost associated with refitting bottom-mounted mooring systems with new batteries (10, 7). The experiment will increase the knowledgebase for the promising renewable energy production source of the SMFC.

Hypotheses

The hypotheses investigated in this study are listed below:

H1. A graphite foam anode will produce more electrical power, per unit volume, than a solid graphite plate anode.

H2. Decreasing the number of graphite plates will decrease the power production of the SMFC.

H3. Decreasing the unit volume of the graphite foam will decrease the power production of the SMFC.

H4. The Geobacteraceae family of exoelectrogen bacteria will be enriched across the volume of graphite foam anode, and the graphite foam with greater porosity will have a greater biomass of Geobacteraceae present.

CHAPTER II

MATERIALS AND METHODS

Sediment Microbial Fuel Cell

The SMFC in this proposed project will be created by using three graphite foam materials (i.e. Duocel® produced by ERG Aerospace, CA and D1-Kfoam® produced by Koopers, PA). The Duocel® foam has two forms listed as 45 pores per inch and 80 pores per inch (ppi). The Kfoam® has an open porosity listed as 70% to 80% porous. All foam porosity will be determined by using the ratio of volume of void space to bulk volume of the foam billet. Using a modified Kimble® 2ml pipette, a dry core sample will be taken from each of the graphite foam sample, and the volume and weight of the sample will be recorded. Using a second pipette, with the bottom sealed, a volume of water will be placed into the pipette and recorded as the initial volume. Then, the core sample will be slid into the pipette containing the known volume of water, so that it is fully submerged. Air bubbles trapped in the foam matrix will be removed by placing a vacuum on the pipette. Once the air bubbles are sufficiently removed, the resulting volume will be subtracted from the initial volume. The pipettes have gradations of 1/100 ml and will be read to the nearest 0.005 ml. If attained, the actual volume of foam will be used to calculate the power produced per unit of the anode. Figure 2 shows an image of the Kfoam® and Duocel® foam billets, and an example of a solid graphite plate.

If the actual volume of the foam cannot be attained using the above technique, then the approximate surface area of the graphite foams as given by the manufacturers will be used. The 80 and 45 pores per inch foams have a given approximate surface area of 5249 m2/m3 and 2624 m2/m3, respectfully (27). Using the nominal pore size of the Duocel® foam, and the approximate surface area of each type, a linear correlation

equation was formed to provide approximate surface area by nominal pore size (See Appendix A). The Kfoam® has a reported nominal pore size of 650 μm (28). The correlation results show the Kfoam® was found to have 1710 m2/m3. The solid graphite plate has a surface area to volume of 966 m2/m3. The surface area of the solid graphite plate (966 m2/m3) is for the resultant surface area for the configuration of the plates in this study, and not a solid cube of graphite. A solid cube of graphite has a surface area to volume ratio of 6 m2/m3.

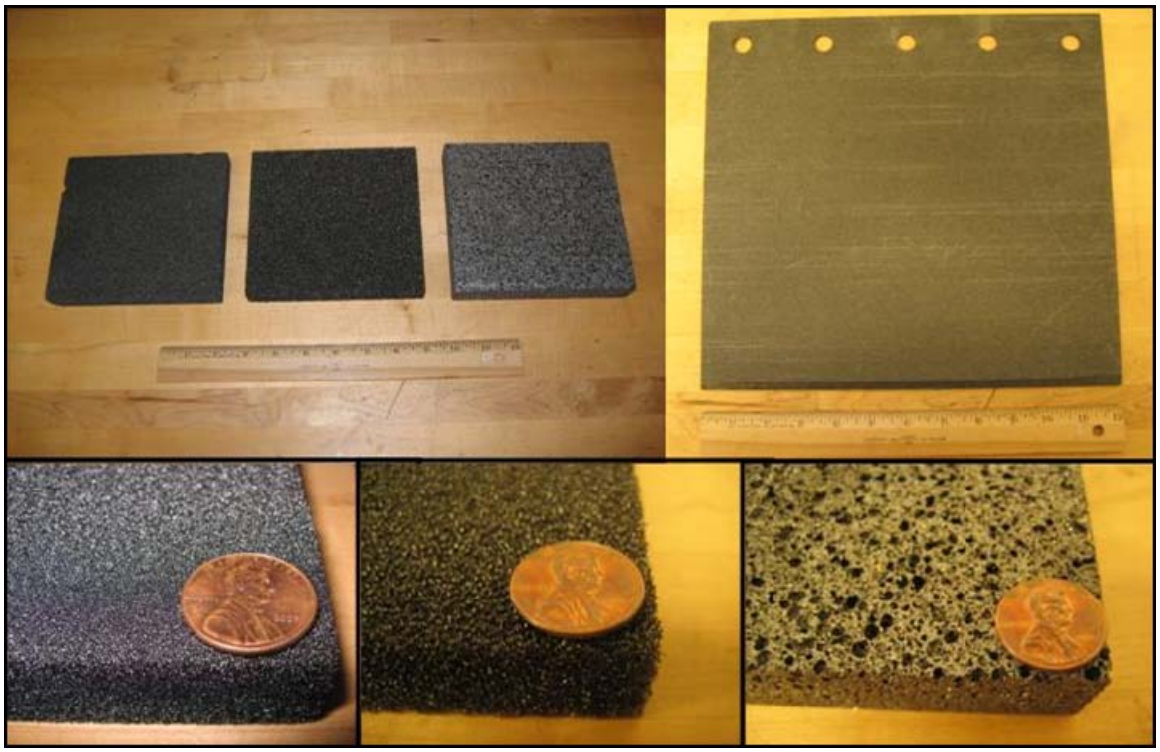

Figure 2. Graphite Foam Billet and Solid Graphite Plate Anode. Top left; Graphite foam billets from left to right, Duocel® foam from ERG Aerospace in 80 and 45 pores per inch, respectively, then the Kfoam® from Koopers, inc are shown. Top Right; a 30.48cm2 graphite plate. This is plate is only an example and not the actual plate used in the study. A standard 12 inch ruler (30.48 cm) is provided for scale. Bottom inset; from left to right, a close up of the 80 and 45 pores per inch Duocel® foams, and the Kfoam®. A penny is provided for scale (1.9 cm diameter).

In this study, all the foam billets are approximately 15.24 cm x 15.24 cm x 2.54 cm cubes, which results in an approximate, bulk-volume of 5.90×10^{-4} m^3. The solid graphite plate is 30.48 cm^2 with a thickness of 0.3 cm, resulting in a bulk volume of 9.2 x

10^{-6} m^3. Using the linear correlation equation found in Appendix A, for each volume used of Duocel® 80 ppi, 45 ppi, Kfoam® and solid plate, the approximate surface area used are 3.1 m^2, 1.5 m^2, 1.0 m^2, and 4.9 x 10^{-3} m^2, respectively. Table one shows a summary of the bulk volume, surface area of the actual amount of anode material used, and the surface area per cubic meter of all anode types.

Table 1

Summary of Graphite Anode Material Volume and Approximate Surface Area

Graphite Type	Bulk Volume (m^3)	Approximate Actual Surface Area (m^3)	Approximate Surface Area per cubic meter (m^2/m^3)
Duocel® 80 PPI	5.9 x 10^{-4}	3.1	5249
Duocel® 45 PPI	5.9 x 10^{-4}	1.5	2624
Kfoam®	5.9 x 10^{-4}	1.0	1710
Solid Plate	5.2 x 10^{-5}	4.9 x 10^{-2}	966

The foam billets were attached to the underside of a 25.4 cm diameter PVC pipe cap. This arrangement provides a stable base for the foam to be attached, isolate the foam anode from the cathode, and also allow for plumbing of the interstitial-water pump. Figure 3 shows a billet of Kfoam® attached to the underside of the PVC pipe cap, with conducting wire and plumbing for water pump attached. The plumbing arrangement draws water from the top center of the foam billet, and in turn, draws interstitial water through the entire foam billet. The peristaltic pump (Masterflex 7550, Cole Parmer, IL) will be set to the lowest speed to draw a consistent flow of water through the plumbing.

The electrical connection is isolated from the water (preventing corrosion) by the use of an epoxy resin (Epo-thin®, Buehler inc., IL).

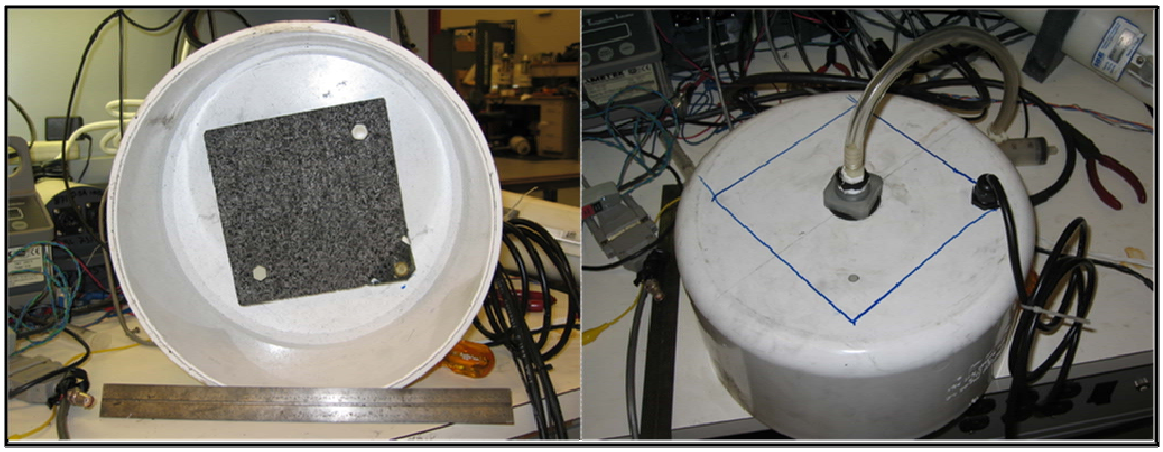

Figure 3. Graphite Foam Billet in Pump Chamber. Left: Image of Kooper Kfoam® installed in the PVC pipe cap. On the lower right hand side of the billet is where the electrical connection was made and isolated from the water with an epoxy sealing compound. Right: Image of the top side of the PVC pipe cap, showing the plumping centered over billet, and the electrical feed through fitting with connecting wire.

The solid graphite plate will be tested by incrementally adding to the surface area of the anode. The solid plate will be divided into three portions and spaced 2.5cm apart when embedded into the sediment test tank. Each of the plates will be incrementally connected and removed from the test circuit, which will enable the test of the second hypothesis (see Figure 4).

The graphite foam billets will be tested individually. Then the foam billet type with the best electrical performance will be tested in the foam-plate configuration (see Figure 4). Three equally sized (nominal, 15.2 cm x 15.2 cm x 0.85 cm) and spaced (2.5cm) foam-plates will be embedded into the sediment test tank. Each of the foam-plates will be connected incrementally increasing the total surface area, and then incrementally reducing the surface area, which will enable the test of the third hypothesis.

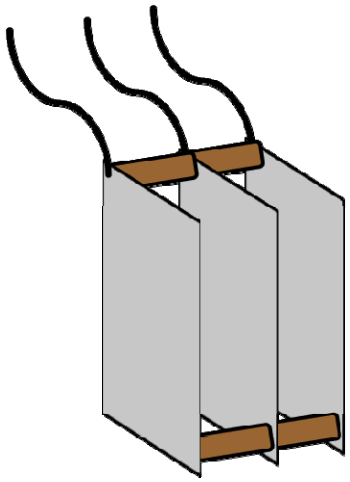

Figure 4. Graphical representation of Plate and Foam Plate Configuration. The grey rectangles represent the graphite anode material, the brown rods are 2.5 cm plastic spacers used to keep the anode spacing consistent during embedment. The black lines on the top represent the electrical connecting wires for each of the anodes

The cathode is a spiral-wound, carbon-fiber "bottle brush", (EG&G, MD) for use in seawater-battery systems. These cathode brushes use titanium metal for the spiral winding of the brush, which reduces the chance of corrosion. The cathode brushes have a diameter of 8 cm with an overall length of 1.0 meters. The surface area of the cathodes has been reported as 26.3 m^2 per meter of electrode length (20). The cathode will be connected to the fuel cell monitoring system through a 1.5 meter, 16 gauge copper wire, with the connection isolated from the water by the use of multiple layers of Scotchweld® adhesive and Super 33+® electrical tape (3M, MN). Figure 5, shows an image of the cathode "bottle-brush".

Figure 5. Left: Graphite carbon bottle brush connected to the conducting wire, Right: Upclose image of large surface area created by the individual conductive graphite fibers. Red scale bar is approximately 2 cm.

Test Tank

The test tank is a glass aquarium that has a 0.42 cubic meter volume. Sediments were collected from the mouth of the Pearl River, in shallow water next to a *Juncus spp.* and *Spartina spp.* bank on August 8, 2007 (30.17893 N, 89.5299 W). The collected sediments had a weight of 280 kg, and had an approximate volume of 0.23 cubic meters. This amount of sediment roughly filled the test tank halfway. The tank temperature will be held constant using a 500 watt tank heater and temperature controller (JH500/JTC, Aquatic Ecosystems, FL). The salinity of the tank water will be held constant by adding synthetic aquarium salt (Instant Ocean®, Spectrum Brands, GA), or topped-off with tap water, when necessary. The physical properties of the tank water were monitored by an Aquatroll®, conductivity and temperature (AT200, In-Situ, CO). The water is oxygenated by the use of two glass air-stones (ALS3, Aquatic Ecosystems, FL), and connected to a compressed air supply. The oxygen content of the water will be periodically measured using a colorimetric, indigo-carmine method (K-7512, Chemetrics, VA).

Scribner Associates 871 Electrical Load Cell

Monitoring of the electrical energy produced will be accomplished by a fuel-cell load testing system (Model 871 fuel-cell monitor, Scribner Associates, Va). The system is capable of monitoring voltage, amperes, 2 Ag/AgCl reference electrodes (Accumet, Cole-Parmer, IL), and temperature. The reference electrodes were placed in the water column and below the sediment, inside the anode chamber. The temperature of the sediment is recorded by the system with the use of a 1 kilo-ohm temperature transducer (AD590KF-ND, Digi-Key, MN). The temperature transducer was potted in the same epoxy resin used to isolate the anode-wire connection. The 871 fuel-cell electronic load system provides an adjustable load for testing various types of small power sources. When there is no load present, the open circuit voltage of the SMFC is a nominal 0.75 volts. When the 871 is instructed to increase the load on the circuit, the circuit is closed and current is able to flow. When the circuit closes, due to the application of the load, a voltage drop occurs. The 871 electronic load system is able to hold the voltage drop to a prescribed level, and the resulting current can be monitored. The 871 electronic load system changes the resistance of the load, to stabilize the voltage of the microbial fuel cell. Figure 6, shows a simplified circuit diagram of the fuel cell and 871 load system. The system monitors the voltage across the load (points A and B in Figure 6), along with the amperes of current. The system is able to log a total of 3000 data points, with an interval of logging between 1 minute and 1 hour. Therefore, with the logging interval at 1 hour, 125 days are able to be recorded, and at the 1 minute interval 2 days of data are able to be recorded.

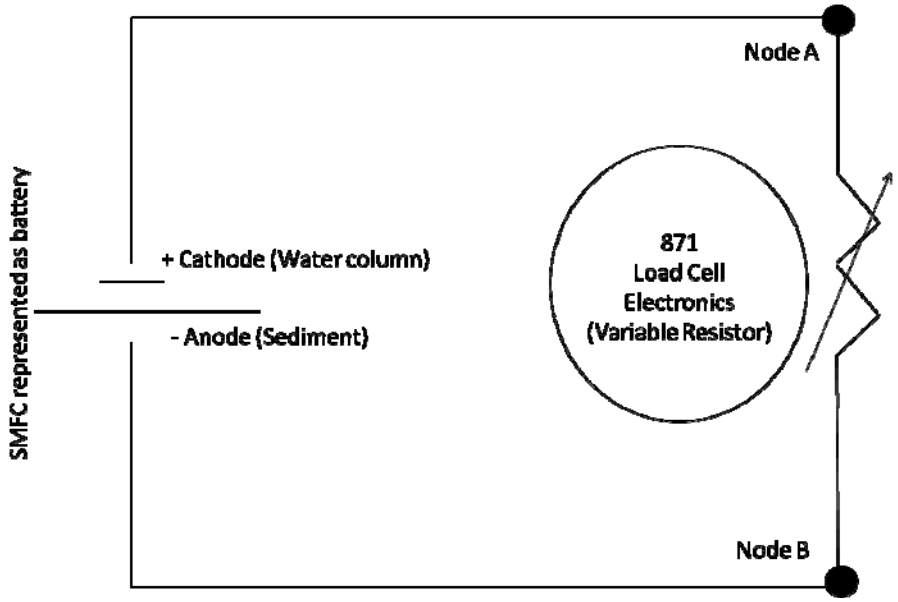

Figure 6. Electrical Diagram of Electronic Load System. This is a circuit diagram of the Microbial fuel cell (represented as a battery), and the 871 Electronic Load cell (represented as a variable resistor). The voltage is monitored across the variable load at points A and B, along with the current.

The data from the Scribner 871 will be input, calculated, and plotted using Microsoft Excel. For each of the anode configurations, plots will be produced to show the polarization curves and power density. Polarization curves are created by plotting cell voltage against current (amperes). For the polarization curve to be produced, starting from the OCV, the voltage of the cell is lowered at a rate of 0.05V per minute to zero, and then raised at the same rate back to the OCV voltage. This technique is also referred to as cyclic voltammetry. The polarization test will occur one day after placing the anode configuration into the test tank. Power curves are found when the power produced by the cell (watts) is plotted against the current (amperes). The power generated is calculated from the formula, where P is power (watts), I is current (amperes), and V is voltage.

$$P = IV$$

The cell will be held at a potential of 0.35 Volts for a minimum of 10 days to observe the persistence of the power produced by the anode. The multiple days may

also allow for colonization of the interior of the graphite foam. After the persistence test is complete, another day will be allowed for the establishment of a pseudo steady state, and then a second polarization test will be performed. Table 2 shows the order of events for the examination of power production using the Scribner 871 electronic fuel cell load system. The final polarization test of the solid graphite plate will have the average of the maximum amps produced, for the scaled down solid plate anodes and a trend line generated.

Table 2

Summary of Electrical Testing Procedure and Durations of Anode Types

Procedure	Duration (Days)
Embed Anode	1
Initial Polarization Tests	2
Persistence Tests	10
Final Polarization Tests	2

Microbial DNA Sampling and Analysis

The experiment will also consist of monitoring the microbial community that is present in the mud, and the biofilm of the anode. The anode microbial community will be monitored for *Geobacteraceae* and the background bacterial load using Real Time Polymerase Chain Reaction (RT-PCR). Following the secondary polarization test, the anode will be gently rinsed with sterile water, and a small core sample of the graphite will be taken using a sterilized stainless steel hole-punch. After extraction from the

anode, the core samples of the graphite foam will be divided into 3 sections (i.e. top, middle, bottom). Five core samples will be taken from the graphite foam billet, one in the center of the billet, and four other samples at a radial distance of 6.5 cm from the center core and ninety degrees apart from one another. Figure 7 shows the pattern for the sample cores and the division of the core into a top, middle, and bottom, with the bottom being towards the sediment. The top, middle and bottom sections will be cut away using a sterile razor blade. The core size will allow for 3 replicate samples from each of the sections. The wet-weight for each sample will be recorded.

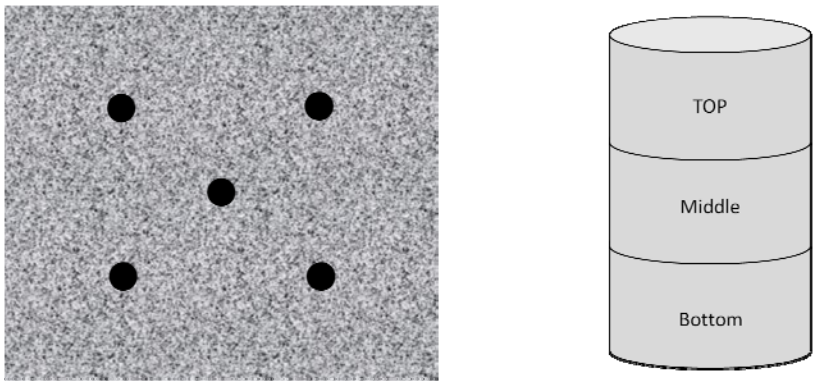

Figure 7. Graphical Representation of DNA Sampling of Graphite Foam Anodes. Left: The core sampling pattern looking at the top of the graphite billet. Right: The division of the sample core, into the top, middle and bottom sections. The top section will be under the PVC pipe cap, and the bottom section will be exposed to the sediment surface

The microbial DNA will be extracted from the graphite by using the ZR soil Microbe DNA Kit ™ (Zymo research Corp., Orange, CA). The protocol from Zymo research will be followed (29). A maximum weight of 0.25 grams per core section will be used for extracting DNA. At the time of sampling the DNA from the anode material, a sample of DNA will also be taken from the test tank sediment. These samples will be used as the control for determining if there was microbial enrichment on the anode above

the amount in the sediment. A field sample, collected from a small bay, outside of the Darling Marine Center, Walpole, Maine, USA, was taken mid November 2010.

Amplification of extracted microbial DNA will be completed using the BioRad IQ 5 RT PCR system. Universal bacterial primers, BACT 1369F and PROK1492R, will be used to amplify the bacterial 16S rDNA constituents of the sediment (30, 31, 32, 5). The universal bacterial primers will have a PCR protocol of the following: initial denaturation step at 94° for 5 minutes, followed by the 50 C_T monitoring cycles at 94° to 57° for 30 seconds dwell at each temperature, and a final melt-curve monitoring cycle from 55° to 95.5° in 0.5° increments, with a dwell time at each increment of 10 seconds. The PCR 16S rRNA amplification for the universal *Geobacteraceae* will include *Geobacteraceae* 494F and *Geobacteraceae* 1050R primers (22). The universal *Geobacteraceae* primers will have a PCR protocol of the following: initial denaturation step at 94° for 5 minutes, followed by the 50 C_T monitoring cycles, dwelling at 94° for 15 seconds, and dwelling for 30 seconds at 61°. The melt-curve monitoring cycle from 55° to 95.5° in 0.5° increments, with a dwell time at each increment of 10 seconds, will be executed. These universal *Geobacteraceae* primers have been shown to amplify DNA extracted from pure cultures of *Desulfuromonas acetoxidans*, *Pelobacter carbinolicus*, *Geobacter sulfurreducens*, *Escherichia coli*, and *Desulfuromusa succinoxidans* (22). The BioRad IQ-5 software will be used to find the relative fold increase or decrease to a control. This will compare the C_T values of the samples, and calculate the relative fold increase or decrease between the sample taken from the anode and the control sample from the sediment. The standard deviations of this relative concentrations are calculated by the IQ5® gene expression software, using the cycle threshold (C_T) values of the amplified targets, and the $2^{-\Delta\Delta\acute{C}T}$ as described in the literature (33, Mark Lawson, pers.

com.). The output of the gene expression software set the sediment control sample at a relative fold value of one, with the rest of the data to be compared to that value. The samples that had values higher than one contained more targeted PCR products than the samples with values less than one, as compared to the tank sediment sample. The C_T values are defined as the replication cycle number for which the fluorescent signal (SYBR green in this study), rose above the background values (relative change in fluorescent units, or RFU), and are inversely proportional to the amount of targeted sample in the PCR well (35). The *Geobacteraceae* primers used in this study were designed to target multiple species of exoelectrogenic microbes (22). Although not mentioned in the Holmes et al. 2004 research, the universal *Geobacteraceae* primer set is highly likely to amplify target 16S rRNA segments of differing size and original concentrations (22, Mark Lawson, pers. com.). This will likely caused a large difference in the C_T values during the PCR process, and will result in large standard deviations during the relative fold comparisons of the PCR data (Mark Lawson, pers. com.).

Gel Electrophoresis

The amplified DNA from the primers will then be put through a Gel Electrophoresis process, which will result in showing the base pair size of the amplicons (16). This will show the different amplicon sizes representing the microbes that colonize the anode material and the surrounding sediment (31). The base pair size of the amplified products should match the size reported for the primers found in the literature (22, 30). Furthermore, comparing the fluorescent intensity of the amplified PCR products to the base-pair size ladder, will allow for an estimate of DNA concentration. Gel Red dye will be used for fluorescent indicator. The gel-electrophoresis will be performed using the BioRad Sub-Cell® GT, horizontal, Agarose Gel Electrophoresis System. Following the

BioRad protocol, a 1% agarose gel and 1x Tris-acetate-EDTA buffer will be used, and will be run for a minimum of 1 hour at 100 volts (26). UV fluorescence imaging of the agarose gel will be performed on the Syngene G-Box system and software. Only the sediment sample with the highest and lowest C_T scores during the PCR procedure will be used for the gel electrophoresis processing. Therefore, for each of the anode configurations, the tank sediment sample and two anode samples will be used in the electrophoresis processing.

CHAPTER III

RESULTS

This study was comprised of two components, the power produced by the sediment microbial fuel cell, and the relative quantification of enrichment for the targeted *Geobacteraceae* species and background bacterial population using PCR techniques and gel electrophoresis. All of the aforementioned graphite anode material types produced electrical power, with varying results. The relative quantification of the *Geobacteraceae* species had mixed results, with only a few of the samples showing increases in relative fold concentrations of targeted species.

Sediment Microbial Fuel Cell Power Production

Physical Properties and Oxygen Content of Test Tank

The physical properties of the test tank were held between 20 – 26 PSU, 19.8 – 20.8 degrees Celsius, and the oxygen was held at or above 8 ppm, during the electrical testing of the anode materials. The highest salinity was found at the end of the Kfoam® experiment, while the lowest salinity was recorded during the 45 pores per inch (PPI) graphite foam. The temperature remained constant for all tests, only fluctuating 1 degree Celsius. The oxygen content of the tank water measured using a colorimetric sample kit was consistently in the 8-10 ppm range of the test kit. Figure 8 is a graph of the recorded physical properties of the test tank. Due to a logging failure of the Aquatroll® data logger, the data presented was taken at the start and end of each electrical test procedure.

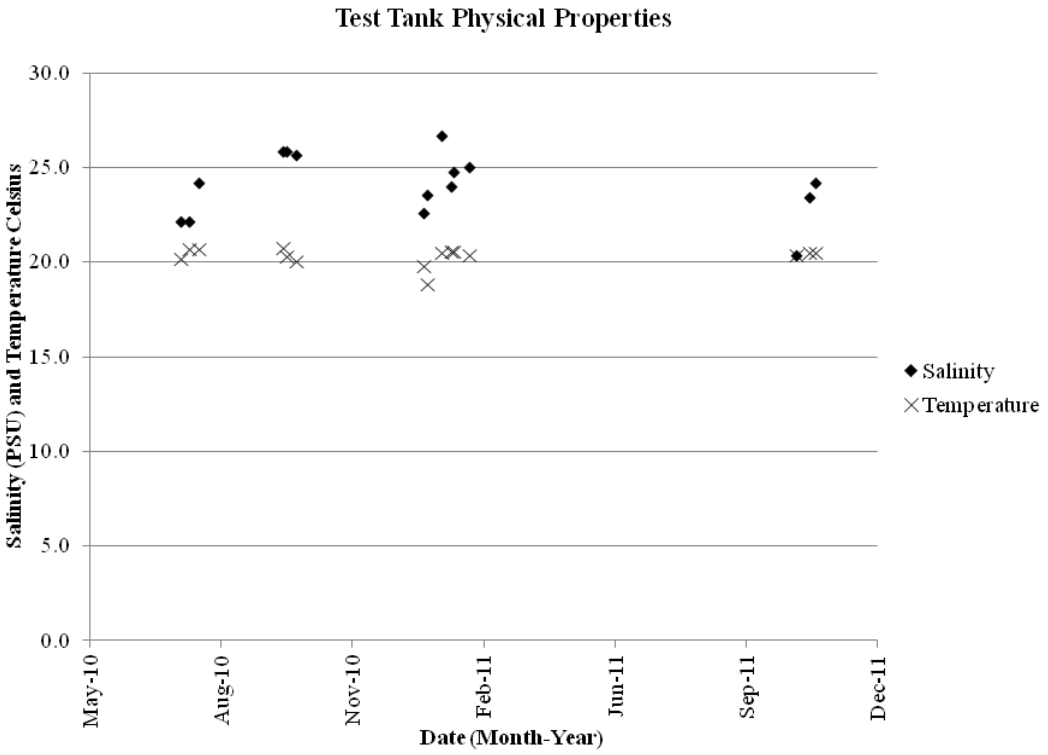

Figure 8. Data Graph of Temperature and Salinity of Test Tank. This shows the Salinity and Temperature data during the extent of the study. "x" are Temperature (degree Celsius) and diamonds are Salinity (PSU).

Approximate Surface Area and Porosity of Graphite Foam Billets

Table 3 shows the results of the approximate surface area calculations for each of the foam types and the solid plate. These volumes were converted to cubic meters and then used to calculate the approximate surface area per billet, using the equation discussed in Appendix A. The anode material that was isolated from the system by insulating epoxy compound was not subtracted from the total. The largest surface area per billet was found with the 80 PPI billet (3.5 m^2), second was the 45 PPI billet (1.5 m^2), and third was the Kfoam® (1.3 m^2). The solid plate has a surface area of 0.1 m^2, which is a total of 3 equally sized plates. The surface area of the bulk volume of the graphite foam anodes was used to normalize the electrical production data.

Table 3

Summary of Approximate Surface Area and Porosity of Anode Material from Volumetric Study

Graphite Type	Bulk Volume (m^3)	Net Volume (m^3)	Standard Deviation (+/- m^3)	Approximate Calculated Surface Area (m^2/billet)	Bulk Volume Surface Area (m^2)	Porosity (%)
80 PPI	3×10^{-7}	5×10^{-8}	0	3.5	6.2×10^{-2}	83
45 PPI	3×10^{-7}	2×10^{-8}	0	1.5	6.2×10^{-2}	93
Kfoam®	3×10^{-7}	9×10^{-8}	1×10^{-8}	1.3	6.2×10^{-2}	70
45 Foam-Plate +	3×10^{-7}	NA	NA	NA	1.55×10^{-1}	93
Solid Plate*	NA	5×10^{-5}	NA	NA	0.1	0

* The solid plate values are the total of 3 equally sized plates. +Foam-Plate values are the total of 3 equally sized pieces. + Foam plate was assumed to have same Net Volume and calculated surface are as 45 PPI graphite foam.

Electrical Power Production of Anode Configurations

In this study, the use of the Scribner 871 electronic load cell was successful in recording the power produced, and allowed cyclic voltammetry of the tested anodes. Anode material testing experiments occurred between July 2010 and November 2011. Table 4 shows the dates experiments were performed, and the physical properties of the test tank. The temperature had no significant deviations, and was held consistently near 20° Celsius. The salinity varied by 4 PSU, with a maximum of 26.7 PSU during the final cyclic voltammetry (CV) test of the Kfoam®. The salinity minimum was 21.3 PSU and occurred during the 45 PPI foam plate test. The solid graphite plate persistence test duration was only 6 days, which was the only test that deviated substantially from the prescribed duration of 10 days. The pump outflow was held at 600 ml / hour for all electrical tests. As table 4 indicates, the 45 PPI graphite foam billet was deemed to have the best electrical performance, and was chosen to be configured in the same fashion as that of the solid plates. The reasons for the choice of the 45 PPI foam as the best performing anode is explained in the discussion session.

The raw electrical power production data produced by the 871 electronic load cell is very large in size, and will only be graphed in this document. Each individual test performed by the 871 electronic load cell produced up to 3000 data points. The 871 electronic load cell data can be requested by contacting the author.

The Relative PCR and gel electrophoresis data is presented in Appendix B through F. The anode sample weight, relative quantity, mean C_T, and Gel concentrations are listed for both the *Geobacteraceae* and bacterial targeted PCR products. The standard deviations for these quantities are also listed in Appendix B through F. The "Gel Note"

column indicates if the sample was used as the high or low concentration for the gel electrophoresis process.

Table 4

Summary of SMFC Power Production Tests, including Dates, Logging Interval, Temperature, and Salinity

Test Name	Start Date	End Date	Log interval (Minutes)	Temperature (°C)	Salinity (PSU)
RYG Plate Initial CV	9-Jul-10	16-Jul-10	1	20.2	22.2
RYG Plate 6 Day*	16-Jul-10	23-Jul-10	1	20.7	22.2
RYG Plate Final CV	23-Jul-10	30-Jul-10	1	20.7	24.2
45 PPI Initial CV	25-Sep-10	28-Sep-10	1	20.8	25.9
45 PPI Ten Day	28-Sep-10	6-Oct-10	5	20.3	25.9
45 PPI Final CV	6-Oct-10	8-Oct-10	1	20.1	25.7
KFOAM Initial CV	10-Jan-11	13-Jan-11	1	19.8	22.6
KFOAM 10 DAY	13-Jan-11	24-Jan-11	5	18.9	23.6
KFOAM Final CV	24-Jan-11	26-Jan-11	1	20.5	26.7
80 PPI Initial CV	1-Feb-11	3-Feb-11	1	20.6	24.1
80 PPI 10 Day	3-Feb-11	14-Feb-11	5	20.6	24.8
80 PPI Final CV	14-Feb-11	17-Feb-11	1	20.4	25.1
45 Foam Plate Initial CV +	22-Oct-11	29-Oct-11	5	20.3	21.3

Table 4 (continued).

Test Name	Start Date	End Date	Log interval (Minutes)	Temperature (°C)	Salinity (PSU)
45 Foam Plate 10 Day +	31-Oct-11	10-Nov-11	5	20.5	23.5
45 Foam Plate Final CV +	5-Nov-11	12-Nov-11	1	20.5	24.2

+ The 45 PPI graphite foam was chosen as the best performing anode material, as explained in the discussion section
* The persistence test for the plate deviated from the methods and was only 6 days in duration..

The experiments listed in Table 4 have been graphed in Figures 9 through 13. The top panel of these graphs show the power produced during the initial CV tests, the persistent power tests (held at 0.35 volt, whole cell potential), and then the final CV test. The power produced was normalized to the square meter of surface area for both the solid graphite plate, and the surface area of the bulk volume of the graphite foam. The bottom panel shows the polarization curves for the each of the graphite types, or configurations. In the case of the solid graphite plates, the first of the final CV test, in which all three sections electrically connected, was used to produce the polarization charts (as indicated in Figure 9). The polarization curve for the 45 PPI graphite foam plate test also used the first of the final CV tests to produce the polarization curve (Figure 13).

The power produced per square meter by the solid graphite plate is shown in the top portion of Figure 9. The surface area that was used to normalize the data was 3.33 x 10^{-2} m^2 per plate. The initial CV tests show the power produced as each of the three solid graphite plates were electrically connected. The first CV test, when only one plate section was electrically connected, was the only CV test that differed significantly from

the rest, and was the lowest at 7 mW/m^2. The subsequent CV tests resulted in power density produced in the 35 mW/m^2 range, with peaks at 42 mW/m^2. The persistence test, between days 6 and 12, resulted in a steady power production of 3 mW/m^2. The final CV tests resulted in peak power density that was lower than the initial CV tests. Starting with all three solid graphite plates electrically connected, the peak power produced was 32 mW/m^2. The peak power density produced with only two plates connected was 27 mW/m^2. The final test with only one plate connected resulted in a peak power density level of 25 mW/m^2.

The polarization curve of Figure 9 was produced from the final CV test, when all three plate sections were electrically connected in parallel. The polarization curve shows 4 separate power cycles. The first of the cycles corresponds with the peak power level, and has peak current of 8.7×10^{-3} amps, corresponding to a voltage range of 0.40 to 0.30 volts. The three subsequent cycles show uniformity, with peak current of 6.9×10^{-2} amps, corresponding with a narrow voltage range of 0.30 to 0.33 volts. As the whole cell voltage drops to zero, the current decreases to 4.2×10^{-3}amps. The voltage increased, from zero to the open circuit voltage of 0.85 volts, caused the current to fall to zero at 0.36 volts for all cycles.

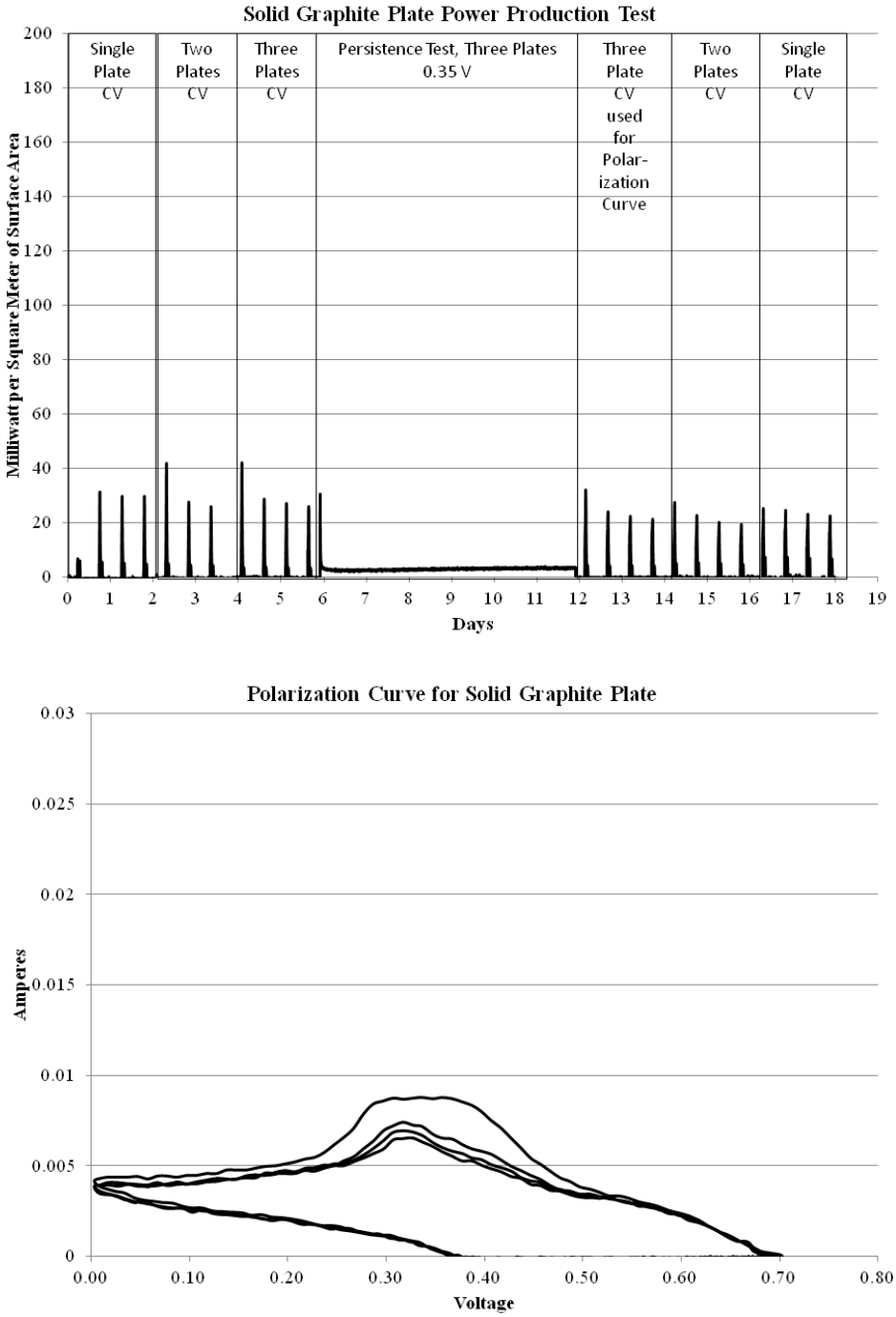

Figure 9. Data Graphs of Electrical Tests of Solid Graphite Plate Anode. Top: CV and persistent power test for the solid graphite plates. Three equally sized plates were used and connected and removed in sequential order. The first CV of all three plates was used to produce the polarization curve on shown below. Bottom: Polarization curve of the first of the final CV tests with all three plates. This graph shows a peak of electrical current at a voltage of 0.35

Figure 10 is the power and polarization graphs of the Duocel® 45 PPI graphite foam. The surface area that was used to normalize the data was 6.2×10^{-2} m^2. The initial CV test resulted in a peak power production of 51 mW/m^2. The persistence test showed a large spike in power produced when the whole cell voltage was dropped from the open circuit value of 0.85 volts down to 0.35 volts (see day 2, Figure 10). The produced power density gradually increased from 15 mW/m^2 during day 2, to a peak of 87 mW/m^2 during days 9 and 10. The produced power density fluctuated 20 mW/m^2 during the last day of the test. The final CV showed a peak power production of 185 mW/m^2 during the final two cycles.

The polarization curve in Figure 10 shows a peak current of 2.3×10^{-2} amps, which corresponded to a narrow voltage range of 0.48 and 0.50. The polarization curve that shows a lower peak current level of 2.0×10^{-2} amps corresponds to the first CV cycle. When the voltage was lowered to zero, the current increased to 2.7×10^{-2} amps. When the voltage was brought back to the open circuit voltage of 0.85 volts, the current fell to zero at 0.63 volts.

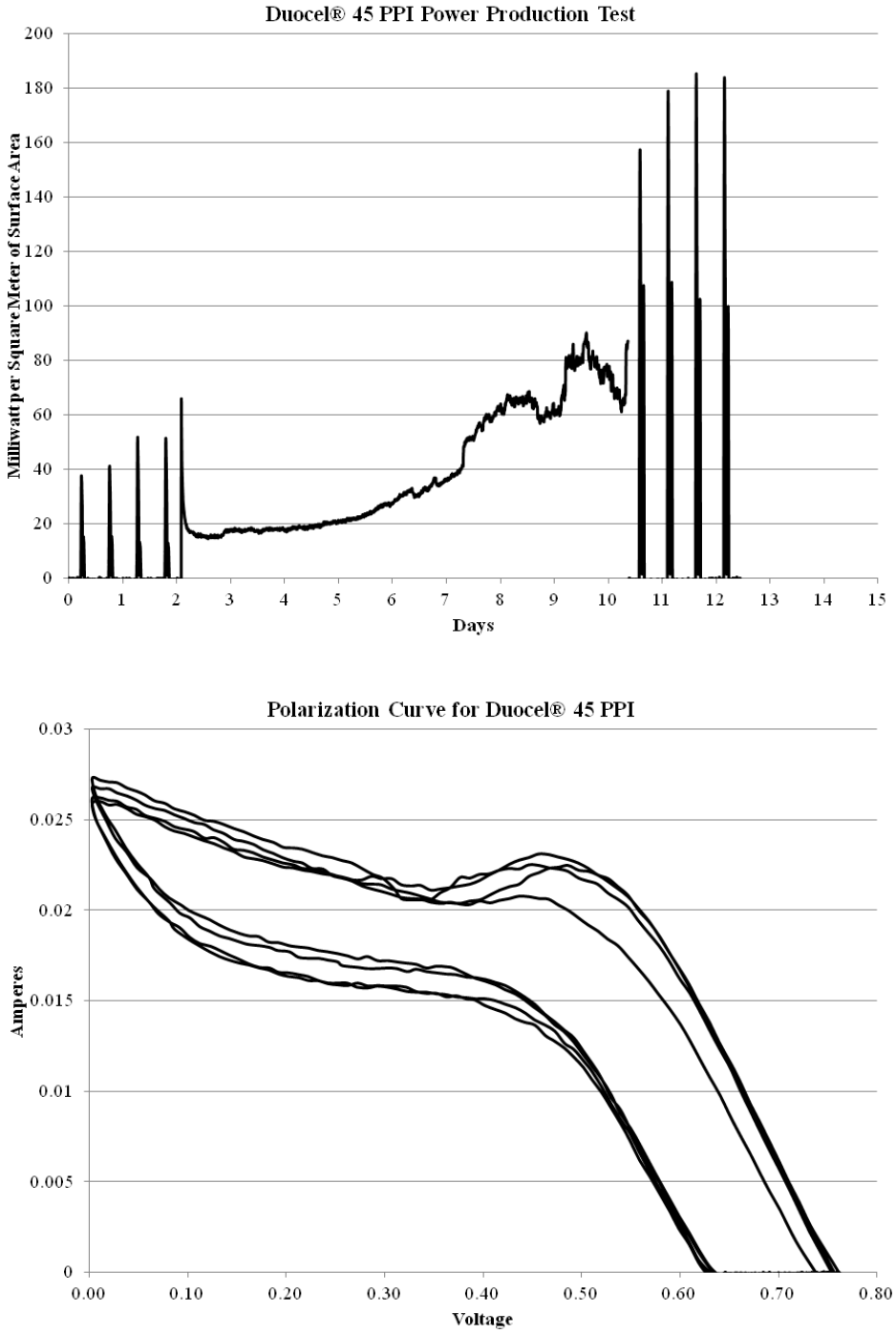

Figure 10. Data Graphs of Electrical Tests of 45 PPI Graphite Foam Anode. Top: CV and persistent power test for the Duocel® 45 PPI graphite foam. Persistent power produced was in the 75-80 mw/m2 range at day 9. Bottom: Polarization curve of the final CV tests. The peak power produced was in the 180 mw/m2 range during the final CV tests.

Figure 11 shows the power production and polarization curve for the Koopers Kfoam®. The surface area that was used to normalize the data was 6.2 x 10^{-2} m^2. The initial CV test did not produce results. The persistent power test gradually increased from 8 mW/m^2 on day 2, to 88 mW/m^2 on day 12. The produced power fluctuated only slightly during the final day of the test. Corrupt data from days 7 through 9 was omitted. Peak power density of 164 mW/m^2 occurred during the first cycle of the final CV test. The subsequent cycles were only slightly lower, but not falling below 160 mW/m^2.

The polarization curve shown in Figure 11, of the Koopers Kfoam®, does not show a unique peak in the data. However, all four cycles are uniform, from the open circuit voltage down to 0.55 volts, and produced a current of 1.9 x 10^{-2} amps. As the whole cell voltage fell to zero, the current produced fell between 1.8 x 10^{-2} and 2.1 x 10^{-2} amps. As the whole cell voltage increased from zero to the open circuit voltage of 0.85 volts, the current produced fell to zero at 0.65 volts for all cycles. The corrupted data in the first cycle was removed, and resulted in the data gap.

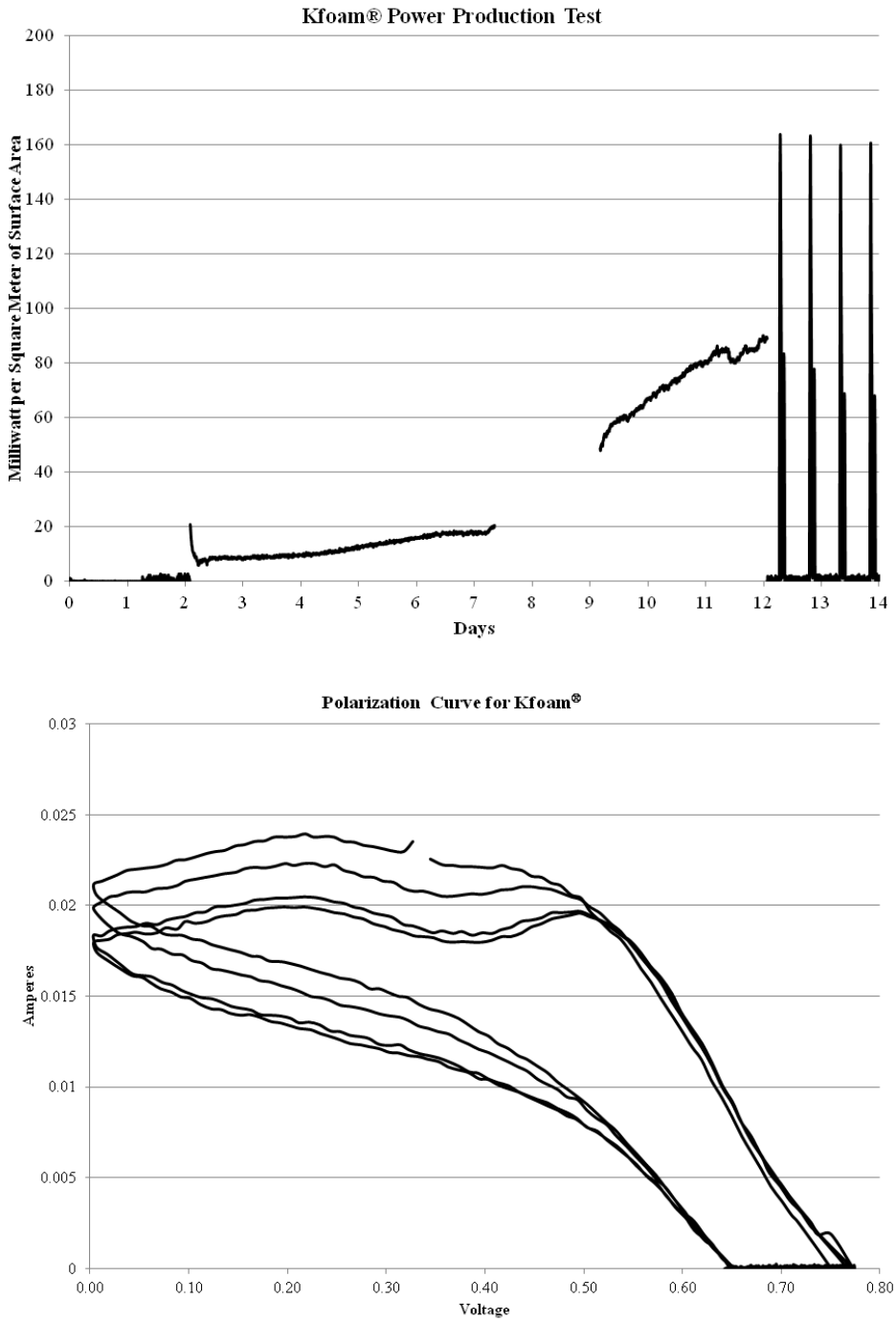

Figure 11. Data Graphs of the Electrical Tests of Kfoam Graphite Foam Anode Top: CV and persistent power test for the Kfoam® graphite foam. The gap in the data was produced from the removal of corrupted data. Bottom: Polarization curve of the first of the final CV tests. This graph shows a peak of electrical current at a voltage of 0.35. Corrupted data was also removed from the first of the 4 CV cycles, and resulting in a small gap

Figure 12 is the power and polarization graphs of the Duocel® 80 PPI graphite foam. The surface area that was used to normalize the data was 6.2×10^{-2} m^2. The initial CV resulted in low power production, with the initial cycle producing a peak at 3.3 mW/m^2. The power production increased during the subsequent cycles, ending at the maximum of 7.8 mW/m^2. The persistence test resulted in a gradual increase in power produced, from 2.5 mW/m^2 to a peak of 32 mW/m^2 during day 9. The final CV test showed similar results to the initial CV test, except the peak values dropped from 9.5 mW/m^2 to 3.2 mW/m^2 during the subsequent cycles.

The polarization curve in Figure 12 is unique, since it does not generate significant current, there is no peak in the data, and the two of the subsequent polarization curves are drastically different. Two of the cycles start producing current when the whole cell voltage passes through 0.38 on the way down to zero. The other two cycles do not start producing current until the whole cell voltage passes 0.15 volts. For all four cycles, as the whole cell voltage reaches zero volts, the current produced is a nominal 5.0×10^{-3} amp. For all four cycles, the current decreases to zero as the whole cell voltage increases from zero to a nominal 0.12 volts.

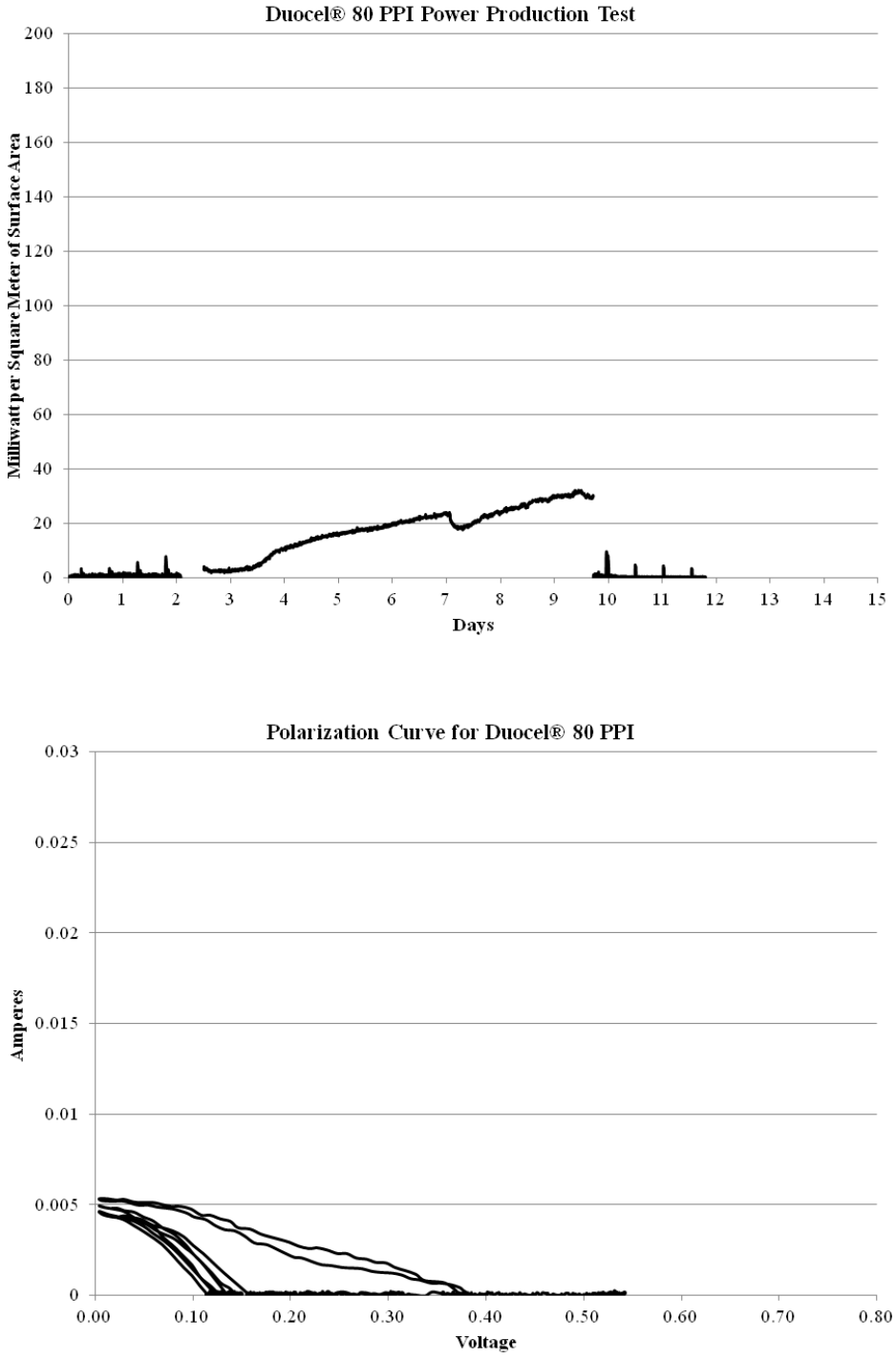

Figure 12. Data Grpahs of Electrical Tests of 80 PPI Graphite Foam Anode Top: CV and persistent power test for the Duocel® 80 PPI graphite foam. Bottom: Polarization curve of the first of the final CV tests. This graph shows a peak of electrical current at a whole cell voltage of zero volts

The power produced per square meter by the Duocel® 45 PPI graphite foam, in the same configuration as the solid graphite plate, is shown in the top portion of Figure 13. The surface area that was used to normalize the data was 5.2×10^{-2} m^2 per foam-plate. The initial CV tests show the power produced as each of the graphite foam-plates were electrically connected sequentially. The first CV test, when only one foam-plate section was electrically connected, had an initial cycle that produced 7 mW/m^2, then the subsequent cycles built up to nominal 15 mW/m^2. Beginning with day 6, the persistence test resulted in fluctuating power production between 10 mW/m^2 and 6 mW/m^2. This range of power production grew steadily to a range of 7 mW/m^2 and 13 mW/m^2. The final CV tests resulted in peak power produced which was higher than the initial CV tests. Initially, all three solid graphite plates were electrically connected in parallel, and the first cycle produced 41 mW/m^2, which increased during subsequent cycles to a nominal 50 mW/m^2. The final test with only one plate connected was not run. The final plate was broken during an inspection of the plumbing.

The polarization curve of Figure 13 was produced from the final CV test, when all three plate sections were electrically connected in parallel. The polarization curve shows 4 separate power cycles. The polarization curve exhibited fluctuation in current when the voltage was decreased from the open circuit voltage of 0.85 volts to zero. For all 4 cycles, when the whole cell voltage reached zero, the nominal current was 1.8×10^{-2} amp. When the whole cell voltage was increased from zero to the open circuit voltage of 0.85 volts, the polarization curve also displayed fluctuations. The current fell to zero, without fluctuation, when the whole cell voltage increased passed 0.65 volts for all 4 cycles.

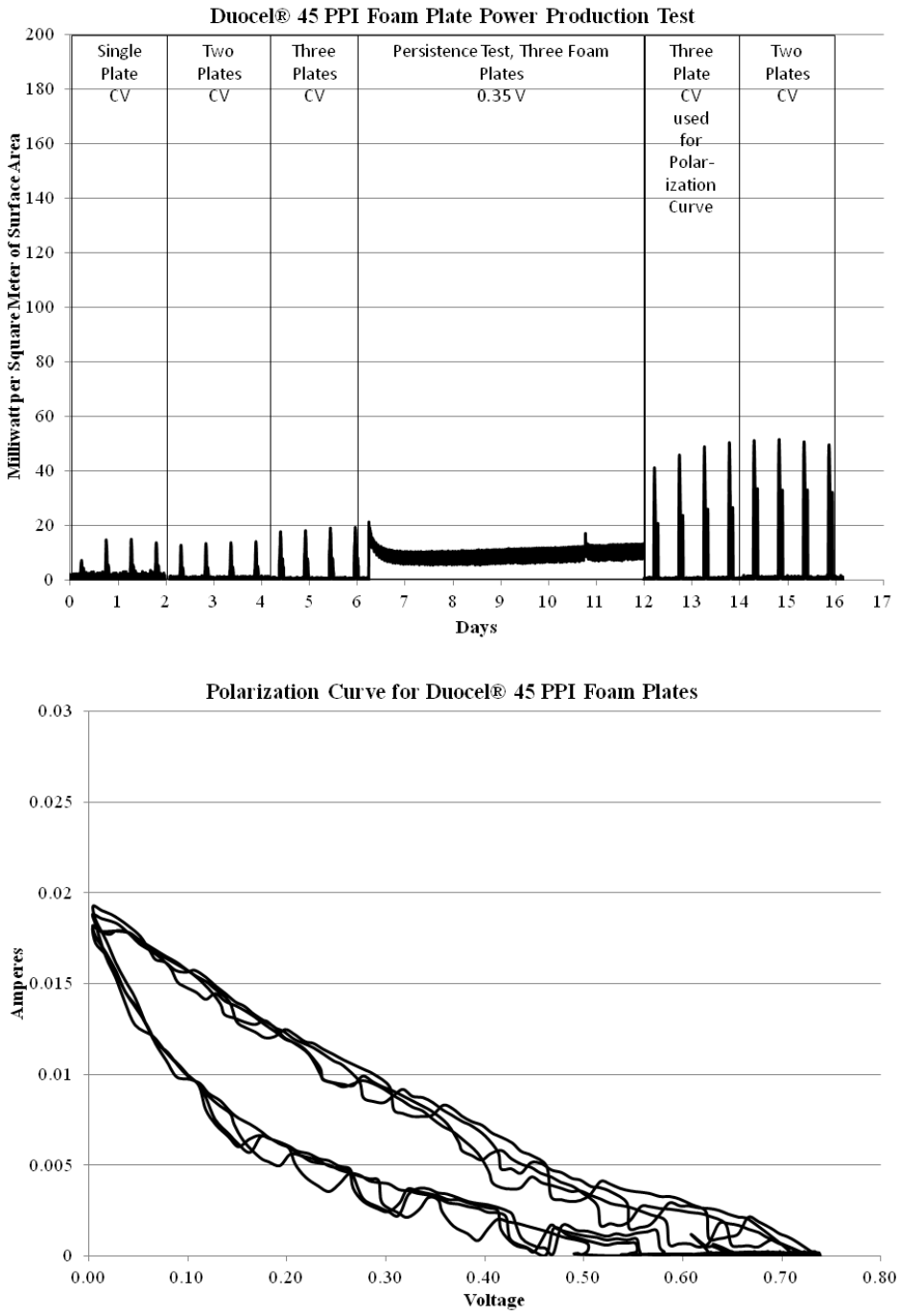

Figure 13. Data Graphs of Electrical Tests of 45 PPI Foam Plate Configuration Top: CV and persistent power test of Duocel® 45 PPI foam in the configured in the same manner as the solid plates. Three equally sized foam plates were used and connected and removed in sequential order. The first of the final CV tests was used to produce the polarization curve. The data during the test was significantly fluctuating. Bottom: Polarization curve of the first of the final CV tests. The noticeable fluctuation can be seen as drops in amperage, and no discernible peak in amperage during the ramping up or down of the voltage cycling

Power Density of Anode Types

The polarization plots in Figures 9-13 show the current produced while the whole cell voltage was incrementally decreased from the open circuit voltage (OCV) of 0.85 volts to zero volts, and then returned to the OCV. This data is converted into a power density curve by calculating the milliwatts per square meter of anode surface area and graphing them versus the whole cell voltage.

Figure 14 shows the power curve for the graphite plate and 45 PPI and Kfoam® anode types. The peaks circled at the top portion of the graph are created when the OCV was decreased to zero during the final cyclic voltammetry tests. The peaks of lower power density (mW/m^2) are created when the whole cell voltage is returned to the 0.85 OCV voltage (lower circle). The solid graphite plate data (black line) follows the same trend as the 45 PPI (blue line) and Kfoam (orange line). Figure 14 shows that while dropping the OCV for 45 PPI foam, Kfoam®, and solid graphite plate the maximum power production (MPP) was at 0.55V, 0.53V, and 0.38V, respectively. The data from the 80 PPI power test (Figure 12), nor the 45 PPI foam-plate (Figure 13) were not included in Figure 14.

Downscaling of Anode Material

Figure 15 shows the maximum amperage that was produced by the solid graphite plate anode, during the final CV tests, as shown if figure 9. Figure 15 plots the actual surface area against the power produced by the subsequent surface area used during the test. The surface area was decreased from 0.1 m^2 for all three plates, 0.07 m^2 for two plates, and 0.03 m^2 for a single plate. Each configuration of anode (triple, double, single) were run through 4 CV tests, and an average amperage was calculated while the voltage was being reduced through 0.5 to 0.2 V, in increments of 0.05 V. This

0.5 to 0.2 region of voltage levels is where the solid plate had an area of maximum production (Figure 9.) This resulted in 30 data points per CV run, then the four CV runs were averaged. The three plate configuration has the highest average amperage produced with 5.6 +/- 0.86 mA. The two plate configuration had an average amperage produced with 3.4 +/- 0.52 mA. The single plate configuration had an average amperage produced with 1.7 +/- 0.05 mA. The resulting linear trendline, equation, and R squared value are reported in Figure 15. A graph was not produced for the 45 PPI foam plate configuration (Figure 13) for reasons explained in the discuttion section.

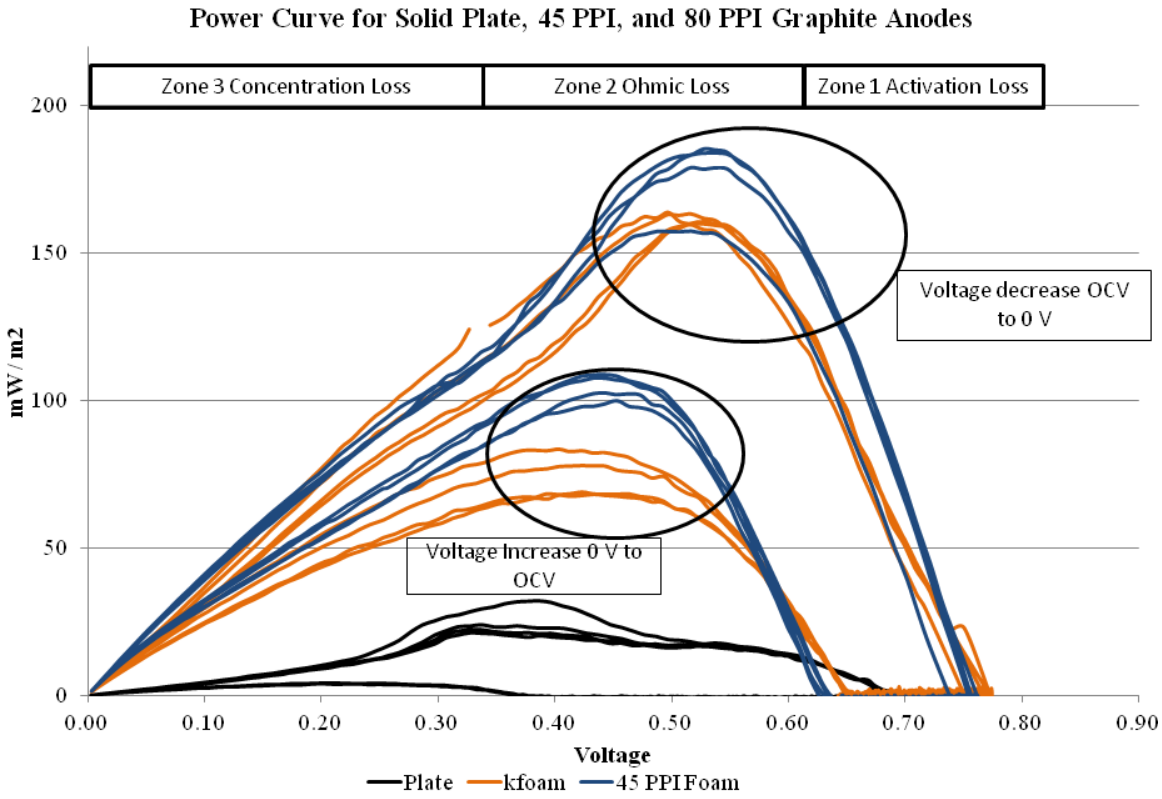

Figure 14. Data Grpahs of Power Density Curves for Faom and Plate Anodes. The comparison of graphite plate, Kfoam®, and 45 PPI anode power density curves. The black line is solid graphite plate, orange line is Kfoam®, and green line is 45 PPI foam anode. The top of the graph shows the three polarization zone model as described by Logan et al. 2006. The zones are approximately placed for reference. The top circle is the peak produced when the whole cell voltage is reduced from open circuit voltage (0.85 V) was reduced to zero. The bottom circle is the peak produced when the whole cell voltage is increase from zero to open circuit voltage (0.85 V).

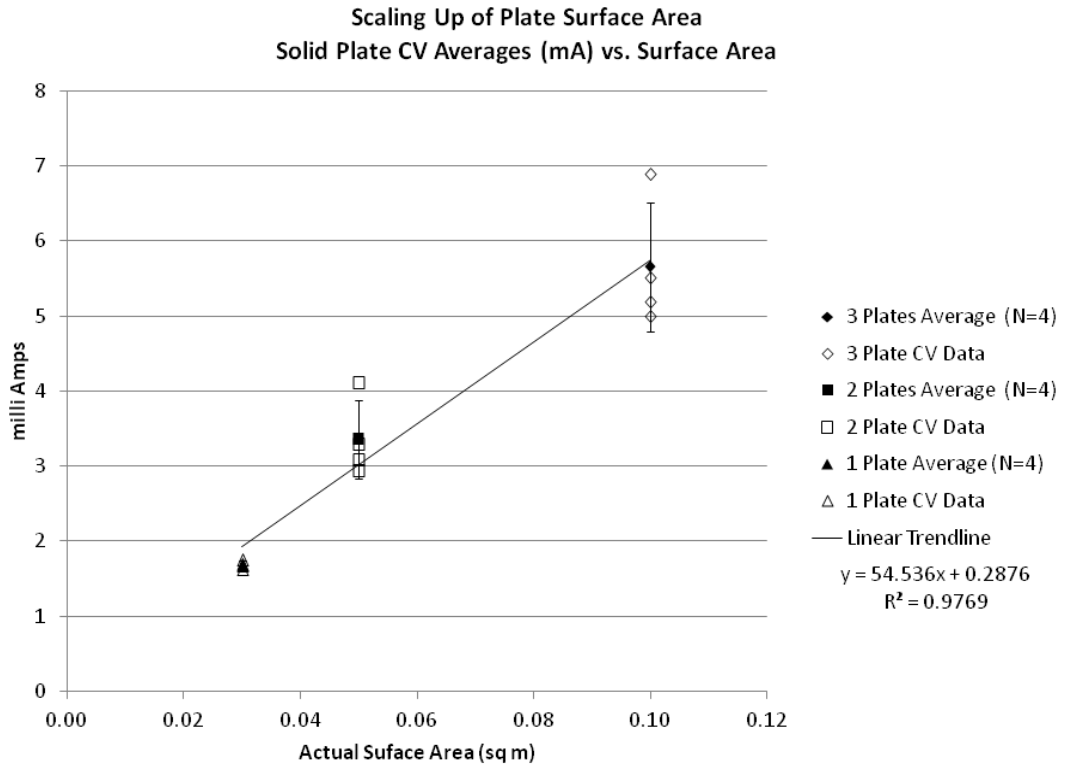

Figure 15. Data Graphs of Downscaling of Solid Graphite Plate. Solid data points are the average of the 4 CV runs, while the open data points show each individual run. Vertical error bars are the standard deviation found. The solid data points were calculated by taking the average of the amperage produced, while the voltage of the CV experiment was being reduced by 0.05V increments, from 0.5 V to 0.2V.

Detection and Relative Enrichment Study of *Geobacteraceae* and Bacterial PCR Targets

A total of 72 DNA samples were extracted from the graphite anode material at the completion of each electrical power production test. The solid graphite plate consisted of 6 samples, where 2 samples were taken from the surface of each of the 3 anode plates. The Kfoam®, Duocel® 45 and 80 PPI foam anodes all had 3 samples taken from each of 5 core samples. This created a total of 15 samples from each of the 3 graphite foam anodes. The Duocel® 45 PPI anode in the foam-plate configuration had 5 samples taken from each of the three foam-plate anodes. At the completion of each test, a sediment sample was collected, which resulted in 5 sediment samples across the time

period of electrical sampling. The complete list of samples, with associated data can be found in Appendix B through F. The sample names indicate where the samples were located on the plate. Sample numbering started at the area nearest the electrical connection, and then proceeded in clockwise around the 6.5 cm radius from the center. The fifth sample was taken from the middle of the foam billets. The solid graphite plate anodes had a sample taken from the top and bottom of each plate. The foam anode that was configured in the plate arrangement followed the same convention as the other foam samples. However, unlike the thicker samples of the full size billets, the thinner sections of foam-plate configuration only provided a single sample for each of the 5 sample sites.

Each group of anode DNA samples and associated sediment samples were extracted and purified using the Zymo Research Soil DNA Mini-Prep™ kit. The purified DNA samples from each anode group were run on a separate PCR well plate, with three replicates for each sample. Each grouping of sampled anode DNA was run through the two separate real-time amplification process. The first RT-PCR amplification was for the "universal" *Geobacteraceae* primer set and the second was run with "universal" bacterial primer set. The sediment samples that were collected during the electrical power tests were also run on a separate PCR plate for both the primer sets, to monitor the sediment for temporal changes.

A relative comparison was performed by inputting the data that was generated during the RT PCR amplification process into the relative gene expression function of the IQ™5 system software. The sediment samples were used as the control for the relative comparison of sample group. The output of the gene expression software set the sediment control sample at a relative fold value of one, with the rest of the data to be compared to that value. The samples that had values higher than one contained more

targeted PCR products than the samples with values less than one, as compared to the tank sediment sample. The relative quantities of targeted PCR products along with the calculated standard deviations are found in Appendix B through F.

Two of the solid graphite plate samples (Yellow Plate Bottom and Green Plate Bottom) and an 80 PPI graphite foam sample (80 PPI 4 Bottom) were destroyed while stored in the freezer. It appears as if the caps were not completely sealed and the frozen sample sublimed. A sediment sample from a field study site at the Darling Marine Science Center, ME was used to compare test tank sediment to an environmental sample (Maine Sed).

Figure 16 shows the relative PCR comparison of the sediment samples taken at the time of the electrical production tests of all anode types and configurations. The initial tank sediment sample was used as the control. The top portion shows the universal *Geobacteraceae* primer targeted samples. All samples were lower in targeted DNA than the initial sediment sample of the tank. The field sample, Maine Sed, was the highest relative concentration, with 0.5 fold below the initial sediment control sample. Error bars on the chart show standard deviation values as calculated by the software. The bottom portion of Figure 16 shows the relative concentrations of the universal bacterial primer targets. The samples were all similar in value, with the values being within 0.25 fold of the initial sediment control. The standard deviations of this data were nominally small.

Figure 17 shows the relative PCR comparison of the solid graphite anode. This anode configuration consisted of 3 individual, equally-sized plate anodes, which were named as red, yellow, and green plates. The ambient sediment sample (Plate Sed) is used as the control. The top portion shows the universal *Geobacteraceae* primer targeted

samples. All samples were lower in targeted DNA than the initial sediment sample of the tank, with the exception of the Green Top sample. This sample showed a 51 fold increase over the control. However, the standard deviation was large for this sample at 44 fold. The bottom portion of the Figure 17 shows the relative concentrations of the universal bacterial primer targets. The universal bacteria targeted samples were all similar in value, with the exception of the Green Top sample, which indicated a 0.4 fold decrease in targets. Except for the Green Top sample data, the standard deviations of the bacterial data were small.

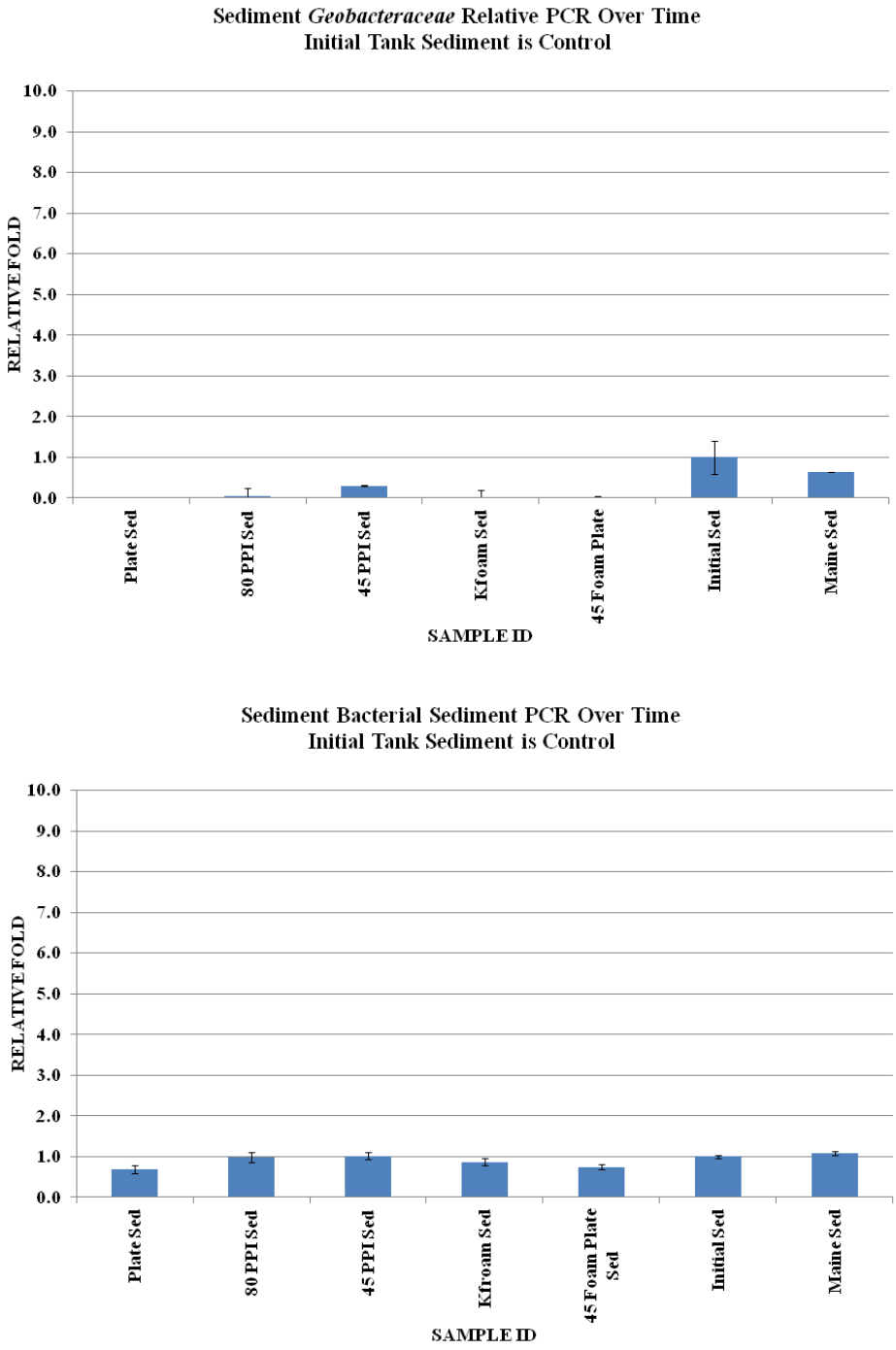

Figure 16. Data Graphs of Relative PCR Comparison of All Sediment Samples. Relative PCR of all sediment samples for both Geobacteraceae (Top) and bacterial (Bottom) primer sets, with standard deviation error bars, using Initial sediment as control. Top: All samples were less relatively less enrichded than control. Bottom: All samples had roughly the same relative amount of bacterial targeted DNA in the samples.

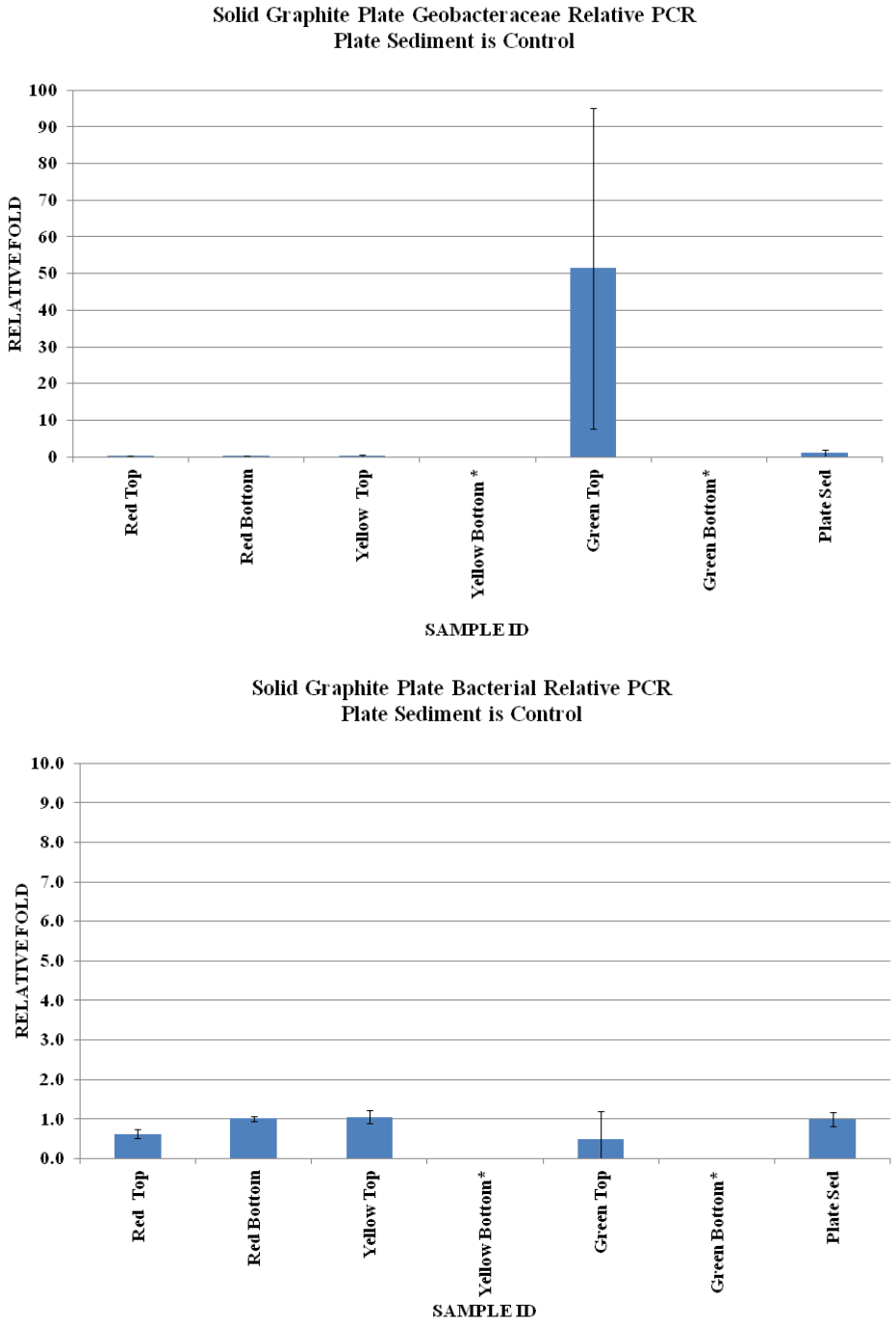

Figure 17. Data Graphs of Relative PCR Comparison of Solid Graphite Plate Anode. Relative PCR of solid graphite plate anode, for both Geobacteraceae and bacterial primers, with standard deviation error bars * Yellow and Green Bottom samples were unavailable. Top: Geobacteraceae relative PCR comparison of plate anode (with large standard deviation). The Green Top sample had 51 fold more targets than sediment control. Bottom: Relative PCR comparison of plate anode using bacterial primers. The Green Top anode sample had 0.4 fold less bacterial targets than the sediment control (with large standard deviation).

Figure 18 shows the relative PCR comparison of the Duocel® 80 PPI graphite foam. The sediment sample taken during this anode test was used as the control. The top portion shows the universal *Geobacteraceae* primer targeted samples. All samples were near zero fold below the level of the sediment control (non-existent). However, sample 4 Top did show 0.3 fold, which was the highest for any of the anode samples in this group. Error bars on the chart show standard deviation values as calculated by the software. The bottom portion of the Figure 18 shows the relative concentrations of the universal bacterial primer targets. All bacterial targeted samples were generally above the level of the sediment control sample. However, most of the standard deviations of the samples overlapped.

Figure 19 shows the relative PCR comparison of the Duocel® 45 PPI graphite foam. The sediment sample taken during this anode test was used as the control. The top portion shows the universal *Geobacteraceae* primer targeted samples. Sample 5 Bottom was a 160 fold increase above primer targets. However, the 5 Bottom sample did have a large standard deviation, with lowest possible value at a nominal 90 fold increase, and maximum at a 250 fold increase above the control. Other samples showed double-digit fold increases, including 1 Bottom, 2 Bottom, 3 Top, 4 Top, 5 Top and 5 Middle. The bottom portion of the Figure 19 shows the relative concentrations of the universal bacterial primer targets. The bacterial primer targets showed similar fold increases, but not in amplitude. Sample 5 Bottom was the largest with a 5 fold increase (+/- 2 fold), followed with 3 Top and 5 Middle showing above 2 fold increases. The 45 PPI graphite foam billet showed the largest fold increase over the control sediment sample for all anode types used in this experiment.

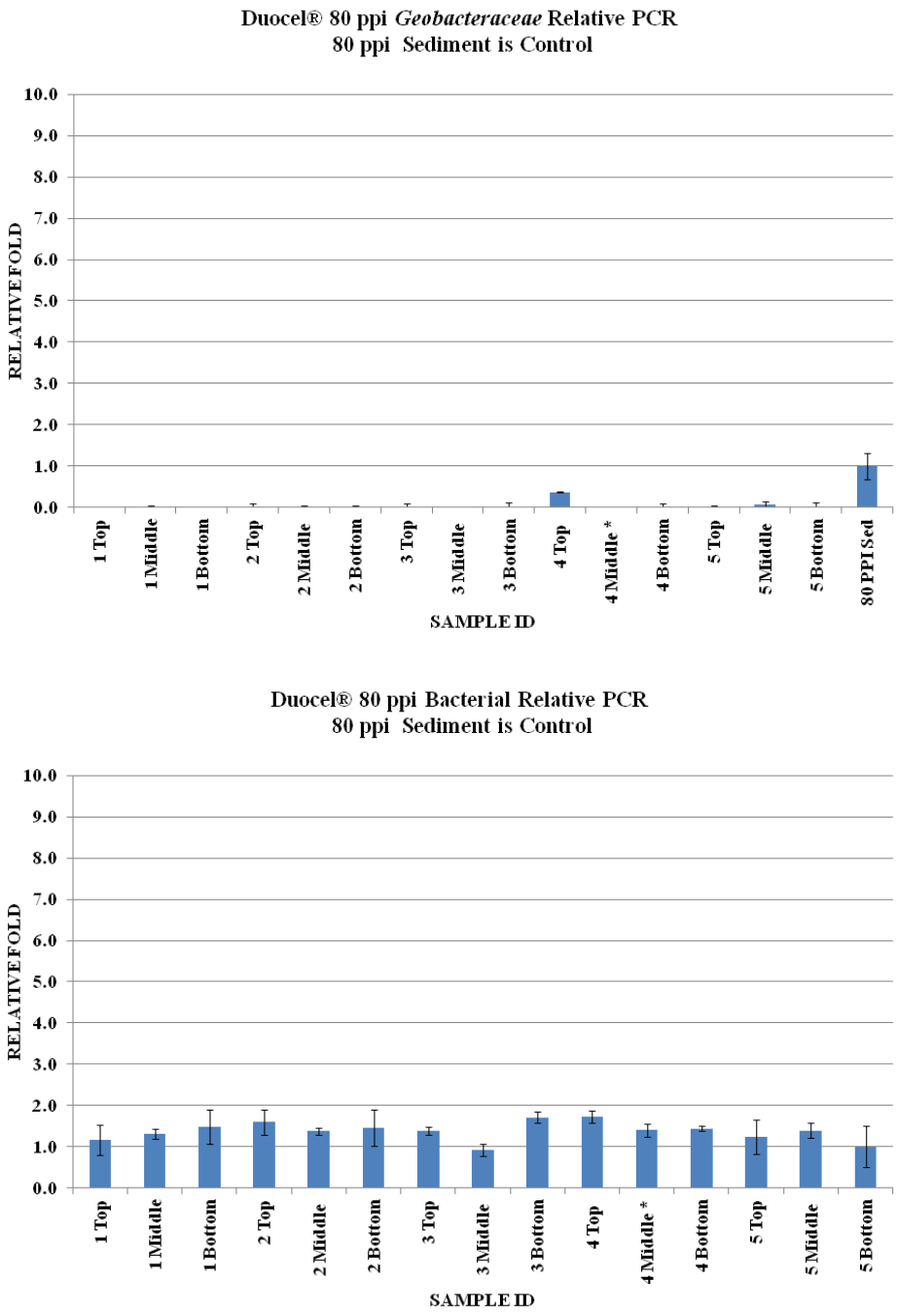

Figure 18. Data Graphs of Relative PCR Comparison of 80 PPI Graphite Foam Anode. Relative PCR of 80 PPI anode, for both Geobacteraceae and bacterial primers, with standard deviation error bars. Top: Geobacteraceae relative PCR comparison 80 PPI anode. The 4 Top anode sample 0.5 fold less Geobacteraceae targets than sediment sample. Bottom: Relative PCR comparison of 80 PPI anode using bacterial primers. Most samples had a fractional fold increases above the sediment control

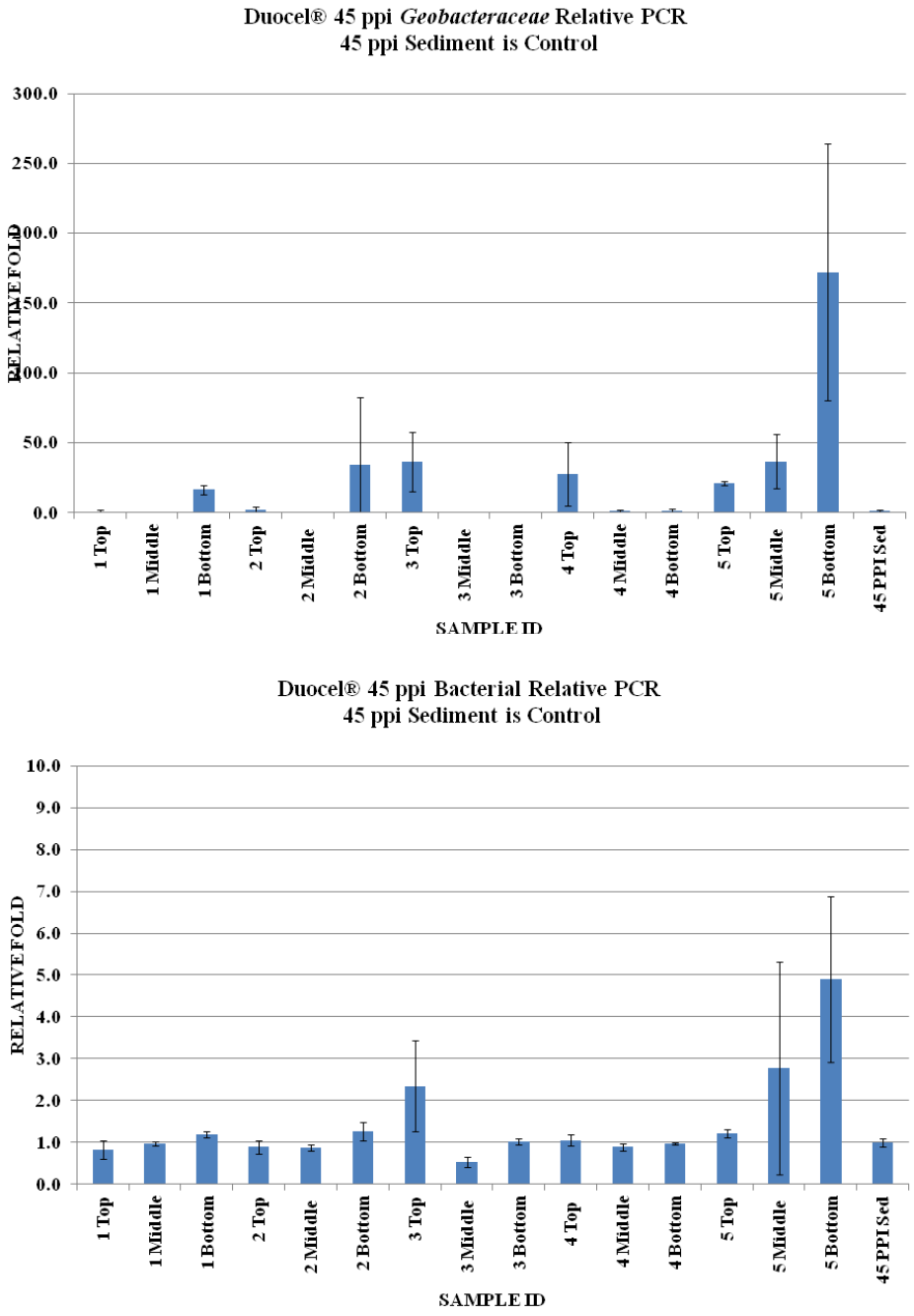

Figure 19. Data Graphs of Relative PCR Comparison of 45 PPI Faom Plate. Top: Geobacteraceae relative PCR comparison 45 PPI anode. 5 Bottom sample had 170 fold increase above control (large standard deviations). Several other samples had 10 fold or above increase above control. Bottom: Relative PCR comparison of 45 PPI anode using bacterial primers. The 5 Bottom sample had a 5 fold increase in the bacterial targets, 3 Top and 5 Middle samples had 2 fold increase above control, but all had large standard deviations. This anode type had the most fold increase of all anode types tested.

Figure 20 shows the relative PCR comparison of the Koopers Kfoam® graphite foam anode. The sediment sample taken during this anode test was used as the control. The top portion shows the universal *Geobacteraceae* primer targeted samples. All samples showed very low levels to non-detected levels of the primer targets. The standard deviations were small for all samples. The bottom portion of the Figure 20 shows the relative concentrations of the universal bacterial primer targets for the Kfoam® anode. The bacterial primer targets for most samples showed values above 0.80 fold, relative to the same amount as the sediment control sample. Samples 2 Top, 3 Middle, and 5 Middle, with relative fold values of 0.62, 0.75, and 0.79, respectively.

Figure 21 shows the relative PCR comparison of the Duocel® 45 PPI foam, configured as the solid graphite anode. This anode configuration consisted of 3 individual, equally-sized plate anodes. These foam anode plates had a similar naming convention, with red white and green used to indicate each individual plate. The ambient sediment sample (45 PPI FP Sed) is used as the control. The top portion shows the universal *Geobacteraceae* primer targeted samples. Two samples, White 2 and Green 5, had a relative fold increase of at 2.6 and 1.9, respectively. Sample Green 2 was relatively equal to the control and the rest of the samples were below the control sample. The bottom portion of the Figure 21 shows the relative concentrations of the universal bacterial primer targets. The universal bacteria targeted samples were all relatively equal to the control sample.

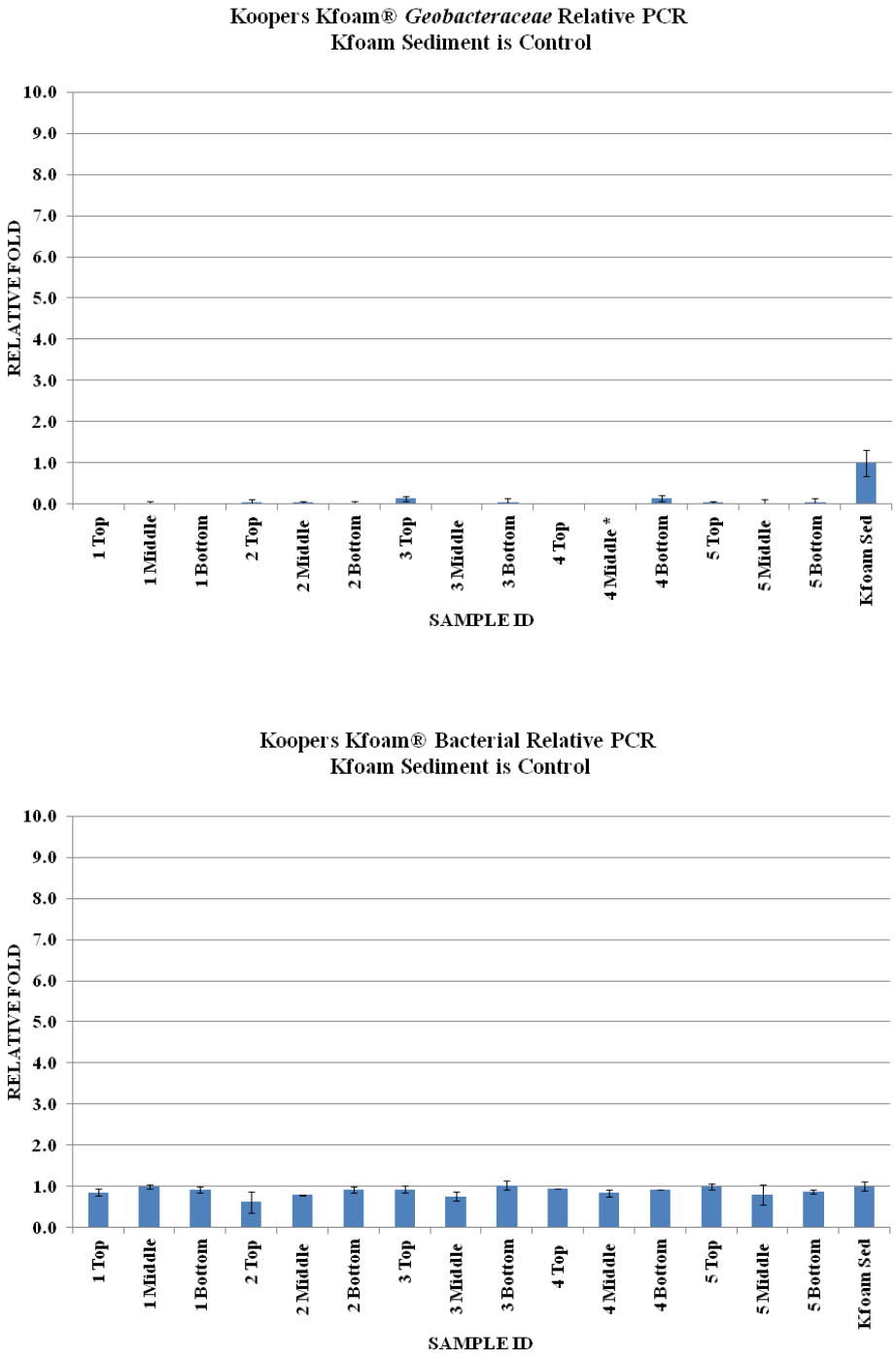

Figure 20. Data Graphs of Relative PCR Comparison of Kfoam Anode. Relative PCR of Kfoam anode, for both Geobacteraceae and bacterial primers, with standard deviation error bars. * 4 Middle has not data available. Top: Geobacteraceae relative PCR comparison Kfoam anode. All samples were well below control. Bottom: Relative PCR comparison of Kfoam anode using bacterial primers. All samples were in the same nominal range as the sediment control sample.

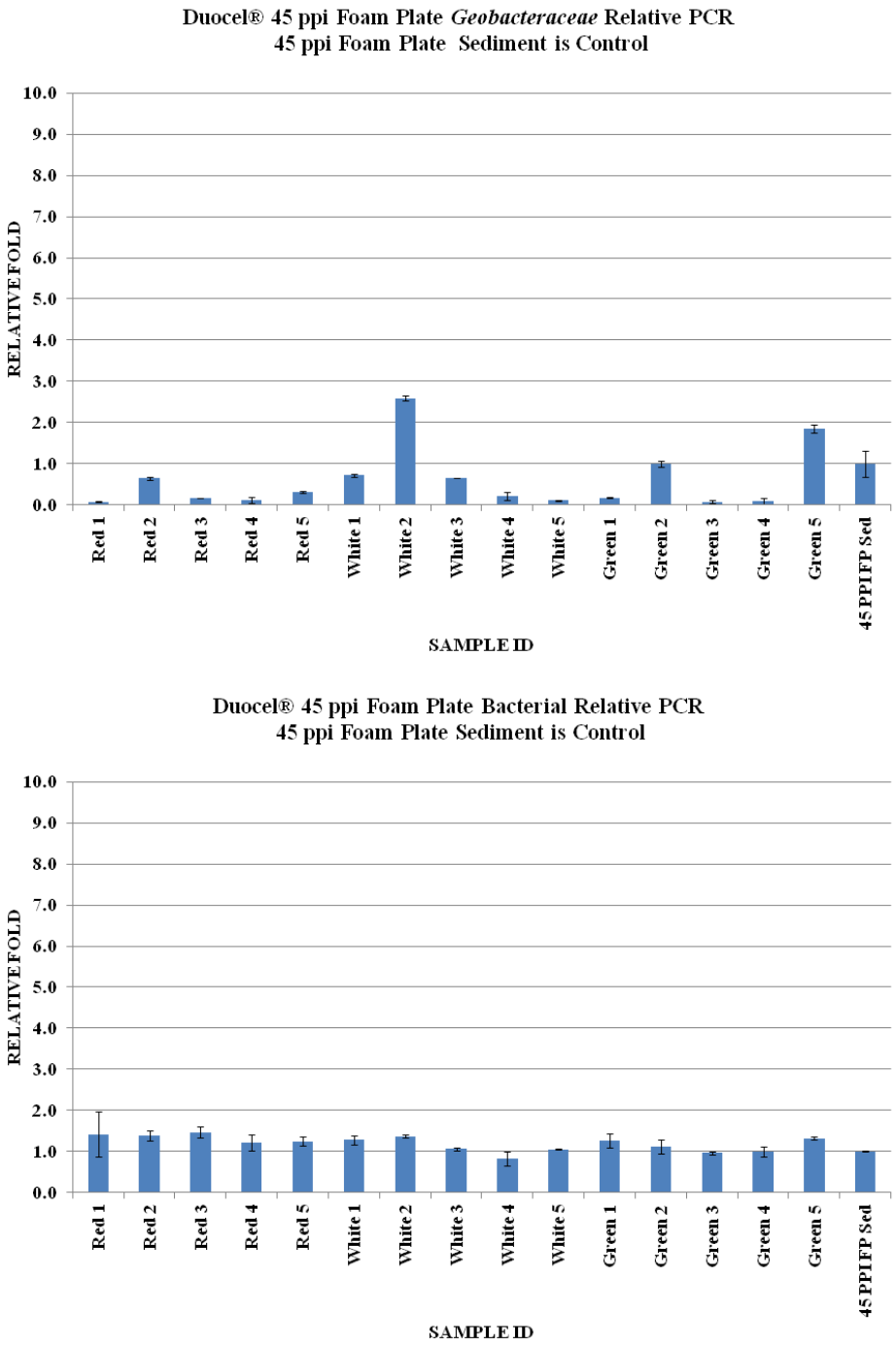

Figure 21. Data Graphs of Relative PCR Comparison of 45 PPI Foam Plate Anode. Relative PCR of 45 PPI Foam Plate anode, for both Geobacteraceae and bacterial primers, with standard deviation error bars. Top: Geobacteraceae relative PCR comparison 45 PPI Foam Plate anode. Samples White 2 and Green 5 were increased over the sediment control. Bottom: Relative PCR comparison of 45 PPI Foam Plate anode using bacterial primers. All samples were in the same nominal range as the sediment control sample.

Figure 22 shows the agarose gel electrophoresis of the Relative PCR amplicons for both the *Geobacteraceae* and bacterial primer targets. The Relative PCR products chosen for the gel electrophoresis technique were the sediment samples taken during each anode electrical test, and the wells that showed the highest increase and decrease relative fold values for each sample group. The electrophoresis was run at 100 volts for 1 hour. The resulting gel was imaged with a centimeter ruler provided on the left side of the gel tray. Low DNA mass ladders were used on either side of the gel, to provide a rough estimation of error. A blank well using sterile water and dye was used to set a zero value. Using the Syngene G-Box software, the concentration of stained DNA was calculated by comparing fluorescent levels of unknown samples to known concentrations of DNA mass ladders. The blue rectangle indicates where the software analysis estimated the concentration of PCR amplicons. The rectangles compare the 800 base pair (bp) standard provided by the low DNA mass ladder. The concentration of the *Geobacteraceae* targets were estimated compared to the 800 bp ladder (20 ng/μL), and the bacterial values were compared to the 100 bp concentration (2.5ng/μL). The blue rectangles indicate the areas that the software scanned to calculate the concentrations of DNA. All results of the agarose gel electrophoresis are shown in Appendix B through F.

The top portion of Figure 22 is the *Geobacteraceae* targeted primer samples. The samples were compared at the 800 bp level, since the highest fluorescent peaks were in this range. Eight of the samples, Kfoam Sed, 80 PPI Sed, 45 PPI 5 Bottom, 45 PPI Sed, 45 Foam Plate Red 1, Initial Sediment, and Maine Sediment had concentrations calculated. The 45 PPI 5 Bottom sample had the highest 800 bp concentration of 206 ng/μL. The lowest concentration at the 800 bp level was the Kfoam sediment sample with 20.5 ng/μL. The blank sample resulted in a concentration of zero,

while the comparison between the mass ladders agreed well with 6 ng/µL difference. The lanes did show some streaking, with more fluorescent peaks occurring at the 100 bp value. The fluorescent peaks in the 100 bp were assumed to be non-specific products, therefore concentrations were not calculated.

The bottom of Figure 22 shows the gel electrophoresis image of samples amplified using the universal bacterial primers. The blue rectangles show the parts of the gel that were compared to provide the concentration as calculated by the software, using the 100bp low DNA mass ladder as a reference. The 45 PPI foam plate sediment sample had the highest concentration of *Geobacteraceae* targets at 182 ng/µL. The 45 Plate White 2 sample had the lowest concentration of universal bacterial primer target concentration of 47 ng/µL. The blank sample resulted in a concentration of zero, and the concentration of the mass ladder lanes, at the 100 bp range, agreed within 1 ng/µL. The lanes showed some streaks starting at the 400 bp level, but the fluorescent peaks were all in the 100 bp range.

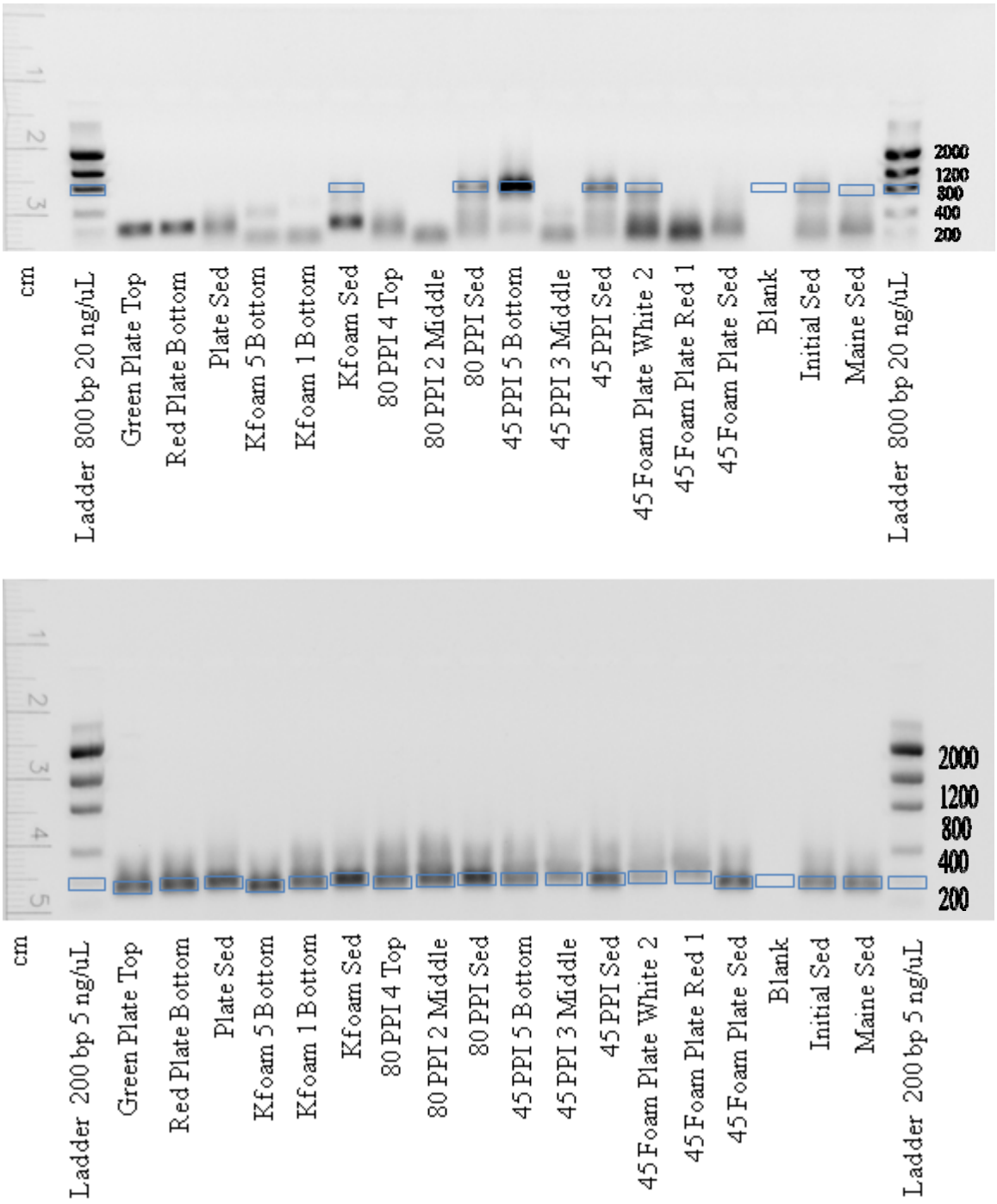

Figure 22. Image of Aragose Gel Electrophoresis of Selected Anode Samples. Gel Electrophoresis of sediment control samples and anode samples that had the highest and lowest amount of targeted DNA detected. Gel was run at 100 volts for 1 hour. On either side is a low DNA mass ladder, which was run twice to provide an estimate of error. Ruler on left side of image is centimeter increments. Blue rectangles indicate areas that were used to calculate concentrations as compared with concentrations of DNA mass ladder. Top: Aragose Gel Electrophoresis of Geobacteraceae primer targets. Bottom: Aragose Gel Electrophoresis of bacterial primer targets.

Figure 23 shows an example of the C_T values found for the 45 PPI graphite foam. These C_T values in Figure 22 were excerpted from the raw data file, and show the difference in C_T values for the relative comparison of samples 5 Bottom (high standard deviation) and 5 top (low standard deviation).

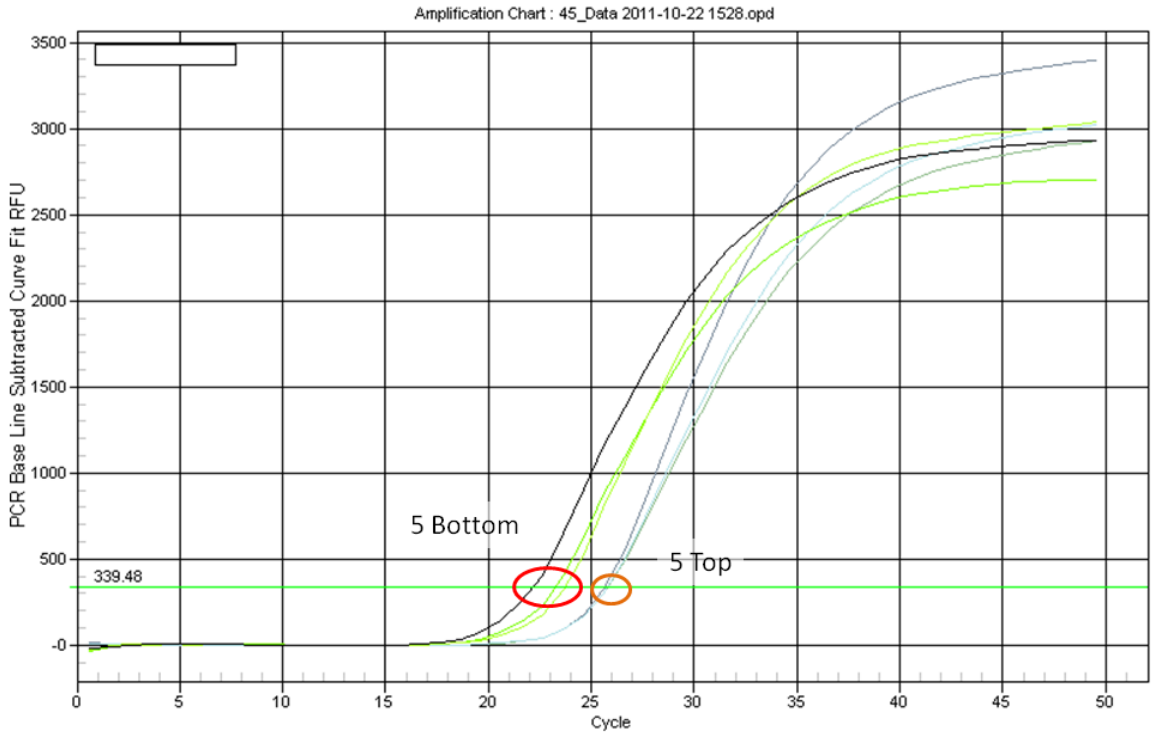

Figure 23. Data Graphs of Selected CT Values of 45 PPI Anode Samples. CT values of 45 PPI samples 5 Bottom and 5 Top. The 5 Bottom sample had a high standard deviation, due to the range of CT values (circled in Red) the standard deviations are large in the relative fold calculations. The 5 Top samples had tightly grouped CT values, that resulted in low standard deviations in the relative fold calculations. The base, background threshold is represented by the green line, and expressed in relative rate of change of the fluorescent signal units (RFU).

The standard deviations for the 5 Bottom were high since the C_T value had a mean reported as 22.75 with standard deviation of 0.77 (Appendix D). The 5 Bottom values of C_T and C_T standard error resulted in a relative fold standard deviation of 91.91 fold (Appendix D). The 5 Top mean C_T value was reported as 21.20, with a standard deviation of 0.09 (Appendix D). Thus, the 5 Top relative fold calculations resulted in a value of 21.20 fold increase with a standard error of only 1.31 fold (Appendix D). This

trend of C_T pattern and relative fold standard errors were found throughout the PCR data set, for both the universal *Geobacteraceae* primer set, and the universal bacterial primer set.

However, the universal bacterial primer set, for the most part, showed much lower standard deviations in the relative fold calculations. This would indicate that the C_T values were more tightly grouped for the universal bacterial primer set. Figures 9-13, previous chapter, show examples of the low values of standard deviation for nearly all samples.

Figure 24 shows the melt curves of the 45 PPI graphite foam anode. The melt curve is formed from recording the relative change in the extinction of the fluorescents of the SYBR green stain, while the temperature is increase (34, Mark Lawson, pers. com.). As the temperature is incrementally increased the PCR products are degraded, and the fluorescence of the stain is extinguished. The top of Figure 24 shows a non-uniform peak in the data, which indicates multiple PCR products created by the universal *Geobacteraceae* primer set. The bottom of Figure 23 shows a distinct peak in the melt curve data, indicating uniform products of the universal bacterial primer set.

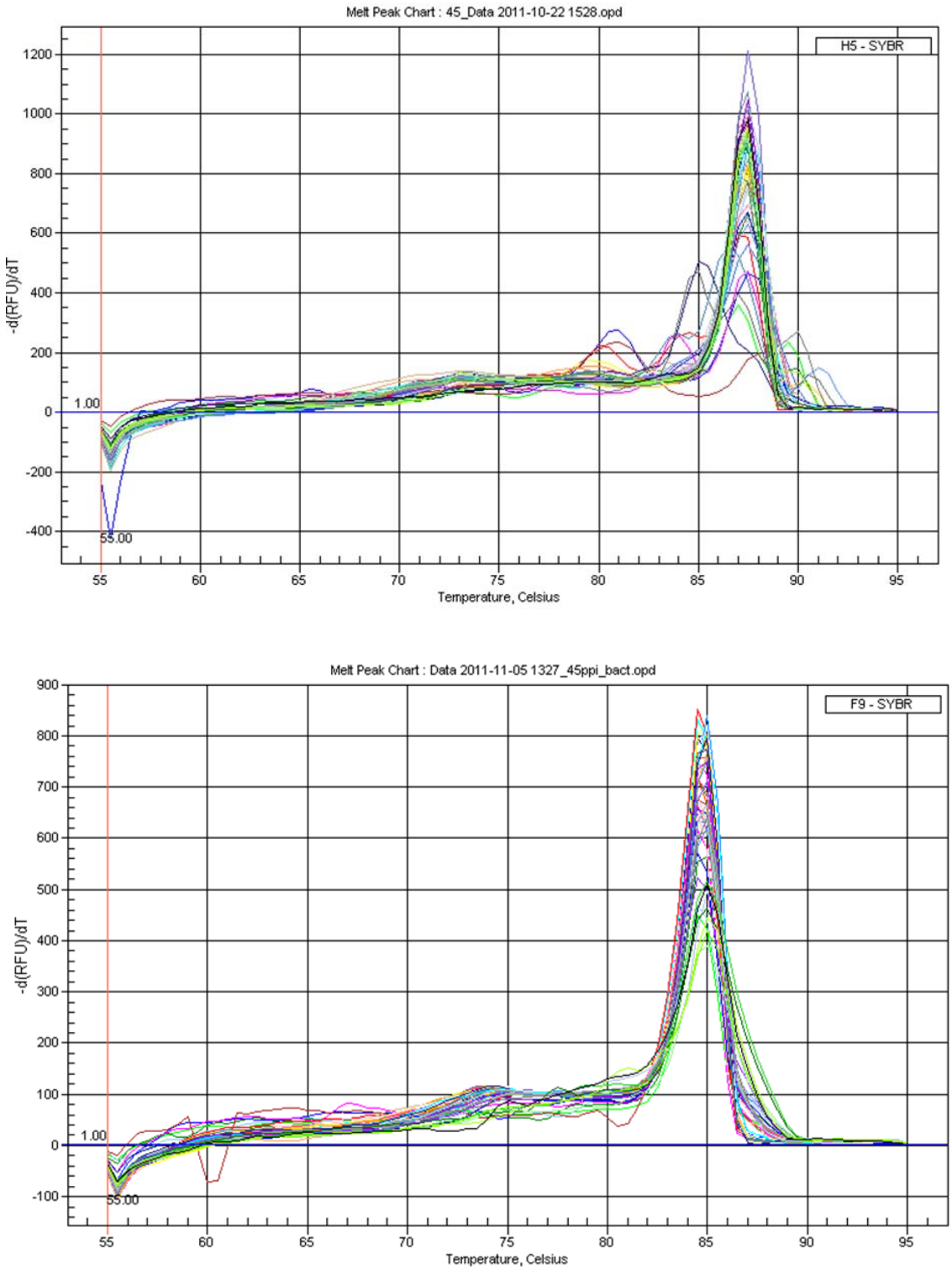

Figure 24. Data Graph of Melt Curves for 45 PPI Anode Samples. Top: Melt peak curve of the universal Geobacteraceae primer set, which shows multiple peaks, indicating multiple PCR products. Bottom: Melt peak curve for the universal bacterial primer set, showing a well formed peak, indicating uniform PCR products

CHAPTER IV

DISCUSSION

The main objective of this study was to test the electrical production of 4 different types of graphite anode material for a sediment microbial fuel cell. The electrical production tests proved successful, and resulted in differences in the amount of electrical power produced by each type of graphite anode material. Normalizing the electrical power production data to milliwatts per square meter, controlling flow of interstitial water through the volume of anode, and stabilizing the physical properties and oxygen concentration of the system allows for inferences to be made about the effective surface area and porosities of the graphite anode types. The agarose gel electrophoresis had results that allow for the base pair comparison of targeted primer amplicons to those found in the literature. The agarose gel electrophoresis also allowed for the calculation of the concentration of PCR amplicons. The procedures in the study allow for a standard comparison method for testing new material or new material configurations for use in a sediment microbial fuel cell.

Sediment Microbial Fuel Cell Power Production

Sediment microbial fuel cells are in the beginning stages, with many research projects aimed at increasing the effectiveness of anode types and or configurations (20, 9). In this study, the most effective anode material found was the Duocel® 45 PPI graphite foam. This anode showed the fastest increase in power production and the highest peak power during CV tests. The power produced by day 9 was over 80 mW/m^2 and the peak power during the final CV was above 180 mW/m^2. The Koopers Kfoam® was a close second, but the power produced by day 9 was lower at 60 mW/m^2, and the peak power during the final CV test was 160 mW/m^2.

The physical properties of the tank were different during the Kfoam® and 45 PPI billet tests. The temperature, oxygen content, and flow rate were the same, but the salinity was different. The salinity during the kfoam® was at 26.7 PSU during the final CV, while the salinity of the 45 PPI billet was slightly lower at 25.7 PSU. A literature review shows that higher salinity will lower the resistivity of the water, allowing for greater power production (36). The Liu et al. 2005, study indicated that the effect of temperature change on the MFC was minimal, with a 12°C temperature drop resulting in a 9% reduction of power produced (36). The higher salinity value during the Kfoam® test shows that the 45 PPI billet was superior, even though the conditions were more favorable for the Kfoam®.

Surface Area and Volume of Anode Material

The 45 PPI foam can be compared to microbial fuel cell power production from the literature. However, there were differences in experimental methods. The differences in reporting the surface area is a place for scrutiny of different reported values of power produced (7).

For example, in an experiment by Nielsen et al. 2007, a sediment MFC was able to produce a nominal 200 mW/m^2 while pumped at a rate of 6.3 ml per minute (20). In the Nielson et al. 2006, experiment, the MFC was configured with a 1 m long carbon fiber bottle-brush for both the anode and cathode. In the Nielson et al. 2006, experiment, the use of the footprint of the MFC was used (0.2 m^2), and not the surface area of the anode itself. De-normalizing the data, by multiplying out the $0.2m^2$ surface area gives 40 mW of power produced by the 1 meter long carbon fiber bottle-brush anode. The carbon fiber bottle-brush has a reported surface area of 26.3 square meters per linear meter, which is 17.5 times the 1.5 m^2 surface area of the 45 PPI foam billet (20, Table 3).

Therefore, if you were to normalize the Nielson et al. 2006, data by dividing the actual surface area of the anode type (26.3 m^2), the result would be 1.5 mW/m^2.

In this study, a nominal 80 mW/m^2 of power was produced from a graphite foam billet with a bulk-volume surface area of 6.2 x 10^{-2} m^2. Multiplying the 80 mW/m^1 by 6.2 x 10^{-2} m^2 results in a de-normalized power production per anode (45 PPI billet) of 4.96 mW. Normalizing this data to the actual surface area of the 45 PPI billet is accomplished by dividing by 1.5m^2 (Table 3), which results in 3.3 mW/m^2. Compared in this manner, the 45 PPI foam billet outperformed the carbon fiber bottle-brush by 1.8 mW/m^2.

Another difference between the Nielson et al. 2006, results and the results of this study is the duration of the experiment. The power production in the Nielson et al. 2006, experiment was started after several weeks of the SMFC being embedded into the sediments. This extended time period above duration of this experiment may have allowed for the further enrichment of exoelectrogens on the surface of the anode (20, 22, 17). According to a study by Mohan et al. 2008, in anaerobic conditions it took 90 days to cover a 7.0 x 10^{-3} m^2 graphite plate with 44% coverage of biofilm, and 180 days to have 96% coverage of the same surface area (36). Converting the Mohan et al. 2008, study to m^2/day resulted in 1.9 x 10^{-9} m^2 per day of biofilm coverage. Assuming this growth rate was linear, to achieve 100% coverage 1 m^2 of solid plate anode would take 19.5 years. This estimated growth rate to cover 1 m^2 of surface area indicates that a significant amount of time should be used to allow for enrichment of anode material with microbial biomass.

A study by Chaudhuri and Lovely 2003, used reticulated carbon foam in a laboratory test using a monoculture of *R. ferrireducens* and produced 6.2 mW/m^2, at 10

days of steady state conditions, using a liquid bath of glucose as the substrate (17). Chaudhuri and Lovley 2005, showed that the graphite foam increased production over solid graphite rods by 2.4 fold, and attributed it to an increase in cells (17). The Chaudhuri and Lovley 2005, study reported the weight of the Pocofoam® graphite foam as 16.4 grams (17). According to the Pocofoam® technical data, this weight would equate to 3.28 x 10^{-5} m^3 of foam (38). The Pocofoam® is reported to have a nominal pore size of 400 μm, therefore, using the equation in Appendix A, the calculated estimate of surface area for Chaudhuri and Lovely 2005, foam anode was 0.14 m^2 (17). If we de-normalize the data in the same manner as above, by multiplying the 6.2 mW/m^2 (power density) by 6.1 x 10^{-3} m^2 (surface area), the result is 3.8 x 10^{-2} mW per anode. Dividing the mW per anode result by the 0.14 m^2 (calculated estimate surface area) the result is 0.27 mW/m^2 for the Chaudhuri and Lovely 2005, foam experiment. The 45 PPI foam in this experiment produced over 12 times the Chaudhuri and Lovley 2005, results, with 3.3 mW/m^2 normalized to the actual surface area of foam present (17). The large difference is inferred to be from the fact that mixed-cultured biofilms have been shown to produce more power (16, 22).

Furthermore, the Chaudhuri and Lovely 2005, study did show that anodes, without bacterial inoculants, did not produce any significant power (17). The lack of microbial growth can be inferred as the reason for the very low power production (near zero) for the Kfoam® and 80 PPI foam used in this study. The fluctuating power production of the 45 PPI foam, configured in the plate arrangement, was assumed to be a plumbing problem, and the sediment-water barrier was periodically shorted and affecting the power produced by the SMFC.

Electrical Power Produced by Anode Types

In Figure 14, zone 1 is described as a steep increase in current as the voltage drops due to activation losses (7). The activation losses can be minimized by the increase of surface area, creating a more rapid increase in power density (7). The increase in the peaks follow the increasing trend of surface area for the three types of anodes compared (table 3). The steep increase is shown as the 45 PPI anode, however, one CV test was very similar to the Kfoam® CV tests. The Kfoam® is less steep than the 45 PPI foam, and has less available surface area per unit volume than the 45 PPI foam. The solid plate has the smallest slope, and has the least amount of surface area. The 80 PPI billet (not shown in Figure 14) has a slope less steep than the plate, but had more surface area. This indicates that an unknown controlling factor was dictating the small electrical output, and shape of the polarization curve for the 80 PPI anode. Zone 2 also shows the voltage at which the maximum power point (MPP) is produced (7).

In Figure 14, zone 2 is the area where ohmic losses are the controlling factor (7). The Kfoam® and 45 PPI graphite anodes show a non-symmetrical semi-circle shape with the dropping of whole cell voltage from OCV to zero (Top circle in Figure 14). In this study, the non-symmetrical curve shape indicates that the SMFC was not being controlled by ohmic losses, but by mass transfer, in the zone 2, while the voltage was being decreased from OCV (7). The bottom circle in Figure 14 indicates the recovery of the whole cell voltage from zero volts to the open circuit voltage. In this study, the power produced when the voltage was being increased from zero to OCV, show a more symmetrical shape. As stated, this more symmetrical shape indicates the ohmic losses are controlling the shape of the curve (7). The power curve for the solid graphite plate

(black) had the most symmetrical semi-circular shape in this study, indicating that ohmic losses were influencing the power density and thus, the shape of the curve.

The third zone in Figure 14 is described as the concentration loss zone, where the mass transport of chemical species, to or from the anode limits the current production (7). This mass transport was attempted to be limited by pumping the interstitial water through the foam, and across the surface of the solid plate. The 45 PPI foam anode (blue line) had the highest power produced in zone 3 of the cell polarization, followed by the Kfoam® (orange line), and lastly was the solid graphite plate (black line). The trend in the data follows the trend of the porosity of the graphite foam, with the Duocel® 45 PPI foam with the highest porosity, next is the Kfoam®, and finally with no porosity is the solid plate.

The 80PPI data is not discussed, since the power curve was well below that of the solid plate, which indicates an unknown influence was controlling the power produced by the 80 PPI SMFC system. Furthermore, the 80 PPI foam did not fall into any of the previously described trends. It is assumed that a short circuit, failure of the pumping system, or clogging of the small pore spaces of the foam influenced the results.

Downscaling of the solid graphite plate anode provided a trend of reduced power production when graphite material is removed from the SMFC system by disconnecting the section of surface area by circuitry and not physically removing it from the test tank. Literature discussing results of a similar test have not been found. In a 2010 article by Wotawa-Bergen, et al, it was stated that more research needs to be done concerning the power production and response of the SMFC system (including environmental response) when shape and size of anodes are modified in scale (40). The downscaling experiment used a small range of surface areas (0.1 to 0.033 m^2) for which a linear trend line was

appropriate for describing. For larger ranges of surface areas, a similar circuitry method could be used, but the mathematics of the trend line will likely be different.

Detection and Relative Enrichment of *Geobacteracea* 16S rRNA Primer Targets

The Relative PCR and Gel Electrophoresis technique was used to detect the relative enrichment of exeolectrogenic species of microbes on the MFC anode types. This techniques is based on the $2^{-\Delta\Delta\acute{C}T}$ method, usually found in gene studies (33, Mark Lawson (BioRad), pers. com., Dr. Joe Griffitt, pers. com.). This technique was performed entirely by the BioRad IQ5® software. The Relative PCR technique was also used to determine the relative concentrations for *Geobacteraceae* specific, 16S rRNA primer targets, for the test tank sediment (and one environmental sample, Maine Sed), over the entire time span of electrical anode testing. Each comparison, for each of the tested anode types, used the sediment as the relative control. The primer set used was created by manual alignment of various gene sequences of exoelctrogenic species by Holmes et al. 2004 (22). This primer set (*Geobacteraceae* 494F and 1050R) tested on a mixture of pure cultured exelectrogenic microbes, such as *Desulfuromonas acetoxidans, Pelobacter carbinolicus, Geobacter sulfurreducens, Escherichia coli,* and *Desulfuromusa succinoxidans* (22).

In this study, sediment samples that were taken during the entire electrical testing period of anode material were compared using the RT-PCR technique (Figure 16, top, Table 4). The control sample for this time series was the initial sediment sample, which was taken prior to the solid graphite plate testing in the beginning of July 2010. The next sample was taken after the solid graphite plate testing concluded at the end of July 2010. The next sediment sample was taken at the completion of the Duocell® 45 PPI foam test, in the beginning of October 2010. The next sediment sampling was at the completion of

the Kfoam® test, at the end of January 2011. After this, the next sediment sample was taken at the completion of the Duocel® 80 PPI foam test, in mid February 2011. The final sediment sample was taken at the completion of the Duocel® 45 PPI foam in the plate configuration in mid November 2011. Samples of the anode material were taken at the completion of each test, along with the sediment samples. The entire time period of the tests was 1 year and 4 months. The relative comparison found in Figure 16, shows that all sediment sample PCR products were lower than the initial sediment sample. The field sample, collected from a small bay, outside of the Darling Marine Center, Walpole, Maine, USA, was taken mid November 2010 (Leonard Tender, pers. comm.) . The relative comparison of the sediment samples show that only the 45 PPI sediment and the field sediment from Maine (Maine Sed) had above zero fold (none detected).

In this study, the only anode types that had significant enrichment of *Geobacteraceae* targets were the solid graphite plate, Duocel® 45 PPI foam, and the Duocel® 45 PPI in the foam-plate configuration. The 45 PPI foam had the greatest enrichment throughout all the samples from all anode types with 172 fold enrichment over the sediment (45 PPI Bottom 5 sample, Figure 19, Appendix D). The other samples from the 45 PPI sample 5 (Middle and Top), also showed enrichments in *Geobacteraceae* specific targets. This would indicate that the exelectrogens were able to colonize through the vertical structure of the foam, and not just along the side that was in direct contact with the sediment. The other samples specific to the 45 PPI anode, 1 Top, 2 Bottom, 3 Top, 4 Top, all had enrichments that were between 15 and 37 fold. The solid graphite plate anode had one sample with a significant increase (Green Top) with 41 fold. The 45 PPI foam, in the graphite plate configuration, had only moderate enrichments of between 2 and 3 fold (White 2 and Green 5, respectively).

The standard deviations of this relative concentrations are calculated by the IQ5® gene expression software, using the cycle threshold (C_T) values of the amplified targets, and the $2^{-\Delta\Delta\acute{C}T}$ as described in the literature (33, Mark Lawson, pers. com.). The C_T values are defined as the replication cycle number for which the fluorescent signal (SYBR green in this study), rose above the background values (relative change in fluorescent units, or RFU), and are inversely proportional to the amount of targeted sample in the PCR well (34). The *Geobacteraceae* primers used in this study were designed to target multiple species of exoelectrogenic microbes (22). Although not mentioned in the Holmes et al. 2004, research, the universal *Geobacteraceae* primer set is highly likely to amplify target 16S rRNA segments of differing size and original concentrations (22, Mark Lawson, pers. com.). This will likely caused a large difference in the C_T values during the PCR process, and will result in large standard deviations during the relative fold comparisons of the PCR data (Mark Lawson, pers. com.).

Agarose Gel Electrophoresis

The results of the gel electrophoresis are shown in Chapter III (Figure 21). For each group of anode samples, the highest and lowest relative fold values were chosen to compare with the gel electrophoresis technique. The universal primer set for the 16S rRNA *Geobacteraceae* targets (Geo 494F and 1050R) had a reported amplicon base pair (bp) size of 500 (22). The universal 16S rRNA bacterial primer sets (Bact 1369F and Prok 1492R) were reported to have an amplicon size of 146 bp (32, 30). The universal *Geobacteraceae* primer set did not show strong fluorescent bands in the 500 bp range, as compared to the low DNA mass ladder (Figure 22, Chapter III). The major bands, especially for the 45 PPI graphite foam sample, 5 Bottom, which had the highest relative fold, were more closely related to the 800 bp size indicated by the low DNA mass ladder.

The bands aligned with the 800 bp level were quantified using the Syngene system software. The bands found below the 800 bp level were not quantified. This difference in bp size ranges of bands implies that multiple PCR products were formed by the *Geobacteraceae* primer set (Mark Lawson, pers. com.). This melt curve results found in Figure 14 are confirmed in the agarose gel results. The top of Figure 24 shows a non-uniform peak in the melt curve data, which indicates multiple PCR products created by the universal *Geobacteraceae* primer set. The universal bacterial primer set showed uniform results in the agarose gel. All of the bands migrated to the 100 bp range of the low mass DNA ladder. The bands were quantified compared to the 100 bp range of the low DNA mass ladder. The uniformity in the bands, is likely from the uniformity in the PCR products base pair size. The distinct peak on the bottom of Figure 24 shows a distinct peak in the melt curve data, which corroborates the finding of the agarose gel electrophoresis process results.

The streaks found in the lanes of the agarose gel (Figure 22) appear for numerous reasons, such as multiple PCR products, high salt content in sample, or impurities in sample, dye, or gel matrix (26, Mark Lawson, per com.). The universal bacterial primer PCR products showed similar streaking to the PCR products from the *Geobacteraceae* primers (Figure 22). The similarities in the gel streaking between the *Geobacteraceae* and bacterial primers may indicate an unknown, systemic-problem with the protocol.

CHAPTER V

CONCLUSION

The hypotheses proposed at the beginning of this document were partially confirmed. The sediment microbial fuel cell that was outfitted with a graphite foam anode produced more electrical power than a SMFC with a solid graphite plate anode. The second hypothesis was confirmed, the data did show a power increase when sections of solid graphite plate anodes were removed from the SMFC. The third hypothesis was not confirmed, the data was not considered viable and did not provide data to make a conclusion. The fourth hypothesis was partially confirmed. The enrichment of the *Geobacteraceae* family of exoelectrogenic bacteria did occur, but it did not occur throughout the entire volume of the graphite foam anode material. The second part of the fourth hypothesis was confirmed; the Duocel® 45 PPI graphite foam anode had the greatest porosity, and was the most enriched in exoelectrogenic bacteria.

The first section of this experiment resulted in a useful data set of sediment microbial fuel cell data, with pertinent information about the comparison of differing anode materials. The graphite foam, while pumped, proved to produce the most electrical power. The benefit of pumping interstitial water through the anode material versus the energy used to pump was not considered in this project. A suggested follow-up study would be to diagnose the most efficient pumping strategy, for the duration and interval necessary to provide adequate mass transport. The future study would investigate the minimum amount of interstitial water to pump, for the most benefit of power production of the sediment microbial fuel cell.

The second part of this study involved Relative PCR and agarose gel electrophoresis to investigate the enrichment of the sediment microbial fuel cell anode by

exoelectrogenic bacteria. The universal *Geobacteraceae* PCR primer set (*Geobacteraceae* 494 F and 1050R) amplified 16S rRNA segments, and thus provided data that indicated enrichment of exoelectrogenic bacteria on the anode material as compared to the exoelectrogenic bacteria found in the sediment (22). The products of the PCR using the *Geobacteraceae* primer set had variable base pair size that were both above (800 bp) the reported value of 500 bp as reported in the literature (22). The enrichment of exoelectrogenic bacteria was not found across the entire volume of anodic material. The universal bacterial PCR primer set (BACT 1369F and PROK1492R) amplified 16S rRNA segments, and produced base pair sized equivalent to that found in the literature (30, 32). The bacterial primer set provided quality data of the relative concentrations of the relative bacterial load for the entire experiment (30, 32).

A recommendation for future studies would be an increase in the duration to allow the slow growth of biofilms across the anode surface (37). A second recommendation for future studies would be to utilize up-to-date technology for identifying and quantifying biological samples, such as the "Next Generation Sequencing" that has recently been developed (39). These sequencing techniques can provide both genomic identification and quantification information for tens of microbial species at a time, thus reducing the workload in the laboratory with an increase in information about the biological samples (39).

APPENDIX A

LINEAR CORRELATION EQUATION FOR ESTIMATED SURFACE AREAS OF GRAPHITE FOAM AND SOLID PLATE

The approximate surface area of the graphite foams as given by the manufacturers will be used. The Duocel® foam in 80 and 45 pores per inch have a given approximate surface area of 5249 m^2/m^3 and 2624 m^2/m^3, respectfully (ERG Aerospace, 2011). Using the nominal pore size of the Duocel® foam, and the approximate surface area of each type, a linear correlation equation was formed to provide approximate surface area by nominal pore size. The Kfoam® has a reported nominal pore size of 650 μm, and this pore size was input into the correlation equation (Koopers, 2009). The equation below, generated from Microsoft Excel was used to calculate the amount of surface area per cubic volume of Koopers Kfoam® graphite foam. The manufacturer did not provide a surface area per cubic volume of the Kfoam®, so correlating it with the Duocel® foam graphite was necessary.

$$\text{Surface Area per Cubic Meter} = -10.626\,x - 8617.8$$

The correlation results show the Kfoam® was found to have 1710 m^2/m^3. The solid graphite plate has a surface area to volume of 966 m^2/m^3.

APPENDIX B

SAMPLE REL-PCR GEOBACTERACEA / BACTERIAL, AND GEL DATA SOLID GRAPHITE PLATE DATA

Core Sample		*Geobacteraceae* Targeted Relative PCR and Aragose Gel						Bacterial Targeted Relative PCR and Aragose Gel					
Sample	Sample Wet Weight (g)	Rel Quant	Rel Quant SD	Mean Ct	Ct SD	GEL CONC ng/uL	GEL NOTE	Rel Quant	Rel Quant SD	Mean Ct	Ct SD	GEL CONC ng/uL	GEL NOTE
Red Plate Top	0.1121	0.1590	0.2028	39.2527	1.8402			0.6281	0.1170	19.9908	0.2687		
Red Plate Bottom	0.1180	0.1455	0.2733	39.3809	2.7101	NA	Gel Low Dimer	1.0176	0.0653	19.2946	0.0925	139.1876	Gel High
Yellow Plate Top	0.1145	0.2859	0.4147	38.4063	2.0925			1.0577	0.1634	19.2389	0.2229		
Yellow Plate Bottom	0.0898												
Green Plate Top	0.1256	51.4346	43.8043	30.9152	1.2287	NA	Gel High Dimer	0.4942	0.7143	20.3367	2.0853	165.6036	Gel Low
Green Plate Bottom	0.1151												
Plate SED	0.2478	1.0000	0.9902	36.5999	1.4286	NA	Gel Sed Dimer	1.0000	0.1745	19.3198	0.2518	120.8874	Gel Sed
Initial Sed (NSS1)	0.2255	99.2355	21.5872	29.9671	0.3138	37.7075	Gel Sed	1.2887	0.1157	18.9539	0.1295	114.1604	Gel Sed

APPENDIX C

SAMPLE REL-PCR GEOBACTERACEA / BACTERIAL, AND GEL DATA

DOUCEL® 80 PPI GRAPHITE FOAM DATA

Core Sample		Geobacteraceae Targeted Relative PCR and Aragose Gel						Bacterial Targeted Relative PCR and Aragose Gel					
Sample	Sample Wet Weight (g)	Rel Quant	Rel Quant SD	Mean Ct	Ct SD	GEL CONC ng/uL	GEL NOTE	Rel Quant	Rel Quant SD	Mean Ct	Ct SD	GEL CONC ng/uL	GEL NOTE
80 PPI 1 Top	0.0797	0.0154	0.0359	36.9448	3.3629			1.1619	0.3642	19.8113	0.4523		
80 PPI 1 Middle	0.0858	0.0078	0.0056	37.9336	1.0344			1.3131	0.1253	19.6348	0.1376		
80 PPI 1 Bottom	0.0732	0.0057	0.0100	38.3862	2.5539			1.4893	0.4204	19.4531	0.4073		
80 PPI 2 Top	0.0238	0.0067	0.0119	38.1534	2.5645			1.5948	0.2948	19.3544	0.2667		
80 PPI 2 Middle	0.0290	0.0004	0.0012	42.2972	4.6898	NA	Gel Low Dimer	1.3771	0.0929	19.5662	0.0974	129.5390	Gel Low
80 PPI 2 Bottom	0.0431	0.0133	0.0066	37.1547	0.7131			1.4689	0.4408	19.4731	0.4330		
80 PPI 3 Top	0.1320	0.0252	0.0114	36.2370	0.6543			1.3818	0.1046	19.5613	0.1092		
80 PPI 3 Middle	0.0399	0.0133	0.0307	37.1534	3.3171			0.9245	0.1423	20.1411	0.2221		
80 PPI 3 Bottom	0.0607	0.0264	0.0214	36.1690	1.1685			1.7148	0.1335	19.2497	0.1123		
80 PPI 4 Top	0.0674	0.3691	0.3019	32.3635	1.1800	NA	Gel High Dimer	1.7331	0.1522	19.2344	0.1267	96.1302	Gel High
80 PPI 4 Middle	0.0350												
80 PPI 4 Bottom	0.0363	0.0086	0.0056	37.7865	0.9348			1.3988	0.1613	19.5436	0.1664		
80 PPI 5 Top	0.0738	0.0005	0.0021	41.9021	5.9658			1.4462	0.0599	19.4955	0.0597		
80 PPI 5 Middle	0.0619	0.0557	0.0229	35.0914	0.5932			1.2502	0.4142	19.7056	0.4780		
80 PPI 5 Bottom	0.0505	0.0197	0.0251	36.5906	1.8369			1.3934	0.1790	19.5491	0.1853		
80 PPI Sed	0.1034	1.0000	0.0959	30.9256	0.1384	50.496	Gel Sed	1.0000	0.5046	20.0278	0.7279	147.8474	Gel Sed

APPENDIX D

SAMPLE REL-PCR GEOBACTERACEA / BACTERIAL, AND GEL DATA

DOUCEL® 45 PPI GRAPHITE FOAM DATA

Core Sample		Geobacteraceae Targeted Relative PCR and Aragose Gel						Bacterial Targeted Relative PCR and Aragose Gel					
Sample	Sample Wet Weight (g)	Rel Quant	Rel Quant SD	Mean Ct	Ct SD	GEL CONC ng/uL	GEL NOTE	Rel Quant	Rel Quant SD	Mean Ct	Ct SD	GEL CONC ng/uL	GEL NOTE
45 PPI 1 Top	0.0573	0.6647	1.2702	30.7696	2.7571			0.6671	1.2778	30.7225	2.7634		
45 PPI 1 Middle	0.0556	0.2296	0.0389	32.3035	0.2443			0.2308	0.0385	32.2539	0.2406		
45 PPI 1 Bottom	0.0728	16.3606	3.1470	26.1482	0.2775			16.3628	3.1008	26.1061	0.2734		
45 PPI 2 Top	0.0881	1.6685	2.2968	29.4419	1.9860			1.6699	2.3044	29.3987	1.9909		
45 PPI 2 Middle	0.0629	0.0219	0.0167	35.6907	1.1003								
45 PPI 2 Bottom	0.0701	33.9502	48.8034	25.0950	2.0739			33.8390	48.5719	25.0578	2.0708		
45 PPI 3 Top	0.0419	36.5115	21.2362	24.9901	0.8391			36.5049	21.2802	24.9484	0.8410		
45 PPI 3 Middle	0.0836	0.0038	0.0073	38.2082	2.7450	NA	Gel Low Dimer	0.0038	0.0073	38.1600	2.7405	63.0854	Gel Low
45 PPI 3 Bottom	0.0803	0.2537	0.2297	32.1594	1.3062			0.2540	0.2287	32.1155	1.2991		
45 PPI 4 Top	0.1520	27.8572	22.6318	25.3804	1.1721			27.9387	22.7103	25.3343	1.1727		
45 PPI 4 Middle	0.1123	1.0300	0.8397	30.1378	1.1762			1.0223	0.8339	30.1067	1.1769		
45 PPI 4 Bottom	0.1181	1.6009	0.8754	29.5015	0.7889			1.5995	0.8645	29.4608	0.7797		
45 PPI 5 Top	0.1637	21.1998	1.3068	25.7744	0.0889			21.4312	1.6026	25.7168	0.1079		
45 PPI 5 Middle	0.1739	36.5322	19.3686	24.9893	0.7649			36.5798	19.5250	24.9455	0.7701		
45 PPI 5 Bottom	0.1576	172.0701	91.9089	22.7535	0.7706	206.8180	Gel High	136.8552	75.6384	23.0419	0.7974	97.1912	Gel High
45 PPI Sed	0.2155	1.0000	0.9217	30.1804	1.3298	69.5322	Gel Sed	1.0000	0.9175	30.1385	1.3237	144.0282	Gel Sed

APPENDIX E

SAMPLE REL-PCR GEOBACTERACEA / BACTERIAL, AND GEL DATA KOOPERS KFOAM® GRAPHITE FOAM DATA

Core Sample		Geobacteraceae Targeted Relative PCR and Aragose Gel						Bacterial Targeted Relative PCR and Aragose Gel					
Sample	Sample Wet Weight (g)	Rel Quant	Rel Quant SD	Mean Ct	Ct SD	GEL CONC ng/uL	GEL NOTE	Rel Quant	Rel Quant SD	Mean Ct	Ct SD	GEL CONC ng/uL	GEL NOTE
Kfoam 1 Top	0.2175	0.0039	0.0096	41.298	3.564			0.8608	0.097	18.822	0.163		
Kfoam 1 Middle	0.1339	0.0280	0.0292	38.444	1.505			0.9903	0.0524	18.620	0.076		
Kfoam 1 Bottom	0.1706	0.0021	0.0025	42.09	1.782	NA	Gel Low Dimer	0.9139	0.073	18.736	0.1154	100.1488	Gel low
Kfoam 2 Top	0.1914	0.0496	0.074	37.620	2.180			0.6212	0.2632	19.293	0.611		
Kfoam 2 Middle	0.1768	0.0408	0.0334	37.903	1.184			0.7962	0.010	18.935	0.017		
Kfoam 2 Bottom	0.2591	0.0306	0.0290	38.319	1.371			0.9165	0.070	18.732	0.109		
Kfoam 3 Top	0.1620	0.1319	0.0568	36.209	0.622			0.9265	0.088	18.716	0.136		
Kfoam 3 Middle	0.1787	0.0028	0.0086	41.787	4.478			0.7581	0.106	19.006	0.201		
Kfoam 3 Bottom	0.1451	0.0453	0.0924	37.750	2.942			1.0259	0.111	18.569	0.156		
Kfoam 4 Top	0.1314	0.0084	0.0175	40.189	3.0243			0.9457	0.011	18.687	0.016		
Kfoam 4 Middle	0.1336	0.0081	00.0167	40.245	2.992			0.8382	0.076	18.861	0.132		
Kfoam 4 Bottom	0.1656	0.1350	0.0792	36.175	0.8467			0.9321	0.0021	18.708	0.003		
Kfoam 5 Top	0.1968	0.0413	0.0319	37.884	1.113			1.0009	0.0778	18.605	00.112		
Kfoam 5 Middle	0.2039	0.0289	0.0803	38.400	4.010			0.7942	0.244	18.939	0.442		
Kfoam 5 Bottom	0.1952	0.0381	0.0935	38.001	3.542	NA	Gel High	0.8822	0.049	18.787	0.081	156.957	Gel High
Kfoam Sed	0.2431	1.0000	0.3158	33.287	0.4556	20.4527	Gel Sed	1.0000	0.109	18.606	0.157	146.623	Gel Sed

APPENDIX F

SAMPLE REL-PCR GEOBACTERACEA / BACTERIAL, AND GEL DATA

DOUCEL® GRAPHITE FOAM –PLATE CONFIGURATION DATA

Core Sample		Geobacteraceae Targeted Relative PCR and Aragose Gel						Bacterial Targeted Relative PCR and Aragose Gel					
Sample	Sample Wet Weight (g)	Rel Quant	Rel Quant SD	Mean Ct	Ct SD	GEL CONC ng/uL	GEL NOTE	Rel Quant	Rel Quant SD	Mean Ct	Ct SD	GEL CONC ng/uL	
F. Plate Red 1	0.1137	0.0727	0.0021	33.177	0.0425		Gel Low Dimer	1.4205	0.5408	18.2471	0.5493	43.0038	
F. Plate Red 2	0.1198	0.6430	0.0762	30.032	0.1710			1.3837	0.1217	18.2849	0.1269		
F. Plate Red 3	0.1399	0.1688	0.0191	31.961	0.1630			1.4675	0.1277	18.2000	0.1256		
F. Plate Red 4	0.1149	0.1213	0.0487	32.438	0.5793			1.2161	0.1931	18.4711	0.2291		
F. Plate Red 5	0.1006	0.3111	0.0432	31.080	0.2004			1.2499	0.1107	18.4316	0.1278		
F.Plate White 1	0.0757	0.7174	0.0812	29.874	0.1633			1.2825	0.1156	18.3944	0.1300		
F. Plate White 2	0.0698	2.5935	0.2262	28.020	0.1258	38.6071	Gel High	1.3662	0.0401	18.3033	0.0423	46.6728	
F. Plate White 3	0.1813	0.6544	0.1080	30.007	0.2382			1.0593	0.0431	18.6702	0.0587		
F. Plate White 4	0.1174	0.2155	0.1177	31.609	0.7883			0.8319	0.1665	19.0189	0.2887		
F. Plate White 5	0.1632	0.1092	0.0400	32.591	0.5293			1.0522	0.0046	18.6800	0.0063		
F. Plate Green 1	0.1581	0.1750	0.0262	31.909	0.2164			1.2719	0.1714	18.4064	0.1944		
F. Plate Green 2	0.0446	1.0000	0.1584	29.395	0.2285			1.1287	0.1719	18.5787	0.2198		
F. Plate Green 3	0.0847	0.0786	0.0094	33.065	0.1722			0.9655	0.0361	18.8040	0.0539		
F. Plate Green 4	0.0771	0.0839	0.0128	32.970	0.2194			0.9917	0.1180	18.7654	0.1717		
F. Plate Green 5	0.2375	1.8537	0.2854	28.505	0.2221			1.3230	0.0314	18.3496	0.0342		
F.Plate Sed	0.212	1.0000	0.0841	29.395	0.1214	NA	Gel Sed	1.00	0.0122	18.7534	0.0177	182.1460	Gel Sed

APPENDIX G

SAMPLE REL-PCR GEOBACTERACEA / BACTERIAL, AND GEL DATA TEMPORAL SEDIMENT SAMPLE DATA

Core Sample		*Geobacteraceae* Targeted Relative PCR and Aragose Gel						Bacterial Targeted Relative PCR and Aragose Gel					
Sample	Sample Wet Weight (g)	Rel Quant	Rel Quant SD	Mean Ct	Ct SD	GEL CONC ng/uL	GEL NOTE	Rel Quant	Rel Quant SD	Mean Ct	Ct SD	GEL CONC ng/uL	GEL NOTE
Plate Sed	0.2478	0.02526	0.01450	33.15	0.8280 1	NA	Gel Sed	0.68196	0.07799	18.66	0.1650	120.8874	Gel Sed
80 PPI Sed	0.1034	0.03509	0.00841	32.68	0.3458 5	50.49580	Gel Sed	0.98789	0.09576	18.12	0.1398	147.8474	Gel Sed
45 PPI Sed	0.2155	0.29630	0.02708	29.60	0.1318 6	69.5322	Gel Sed	1.01989	0.05985	18.08	0.0847	144.0282	Gel Sed
Kfoam Sed	0.2431	0.02420	0.00679	33.21	0.4049 9	20.4527	Gel Sed	0.87182	0.05033	18.30	0.0833	146.6230	Gel Sed
Foam Plate Sed	0.2120	0.01878	0.00558	33.58	0.4289 4	NA	Gel Sed	0.74256	0.05626	18.53	0.1093	182.1460	Gel Sed
Initial Sed (NSS1)	0.2255	1.00000	0.40580	27.84	0.5854 5	37.7075	Gel Sed	1.00000	0.03310	18.11	0.0478	114.1604	Gel Sed
Maine Sed	0.2243	0.63321	0.16650	28.50	0.3793 5	NA	Gel Sed	1.08528	0.08506	17.99	0.1131	91.073	Gel Sed

REFERENCES

1. Davis, J.B. and H.F. Yarbrough, Jr. Preliminary Experiments on a Microbial Fuel Cell. *Science*, 1962 137:3530 615-616.
2. Logan, B.E., J.M. Reagan. Microbial fuel cells – Challenges and applications. *Environ Sci Technol.* , 2006 **40:** 5172-5180.
3. Booki, M. J. Kim, S. Oh, J.M. Regan, B.E. Logan. Electricity Generation from swine Wastewater using Microbial Fuel Cells. *Water Res.,* 2005. 39:4961-4968
4. Da Silva, M.L.B. and P.J.J. Alvarez. Enhanced Anaerobic Biodegratdation of Benzene-Toluene-Ethylbenzene-Xylene-Ethanol Mixtures in Bioaugmented Aquifer Columns. *Appl. Environ. Microb,.* 2004. 70(8): 4720-4726.
5. Da Silva, M.L.B, R.L. Johnson, and P.J.J. Alverez. Microbial Characterization of Groundwater Undergoing Treatment with a Permeable Reactive Iron Barrier. *Environ. Eng. Sci*., 2007 24(8): 1122-1127.
6. Lovley, D.R., Microbial fuel cells: novel microbial physiologies and engineering approaches. *Curr. Opin. Biotech*., 2006 . 17: 327-332.
7. Logan, B.E., B. Hamelers, R. Rozendal, U. Schroder, J. Keller, S. Freguia, P. Aelterman, W. Verstraete, K. Rabey. Microbial Fuel Cells: Methodology and Technology. *Environ Sci Technol.,* published online July 2006.
8. Rabaey, K., G. Lissens, and W. Verstraete, in *Microbial fuel cells: performances and perspectives. Biofuels for fuel cells*: biomass fermentation towards usage in fuel cells. IWA Publishing, London, UK. 2005
9. Delong, E.F., P. Chandler, Microbially Powered Fuel Cells Tap Into an Abundant Ecosystem Energy Circuit. *Nat Biotechnol.,* 2002. 20: 788-789. Published online August 2006.

10. Regeura, G., K.P. Nevin, J.S. Nicoll, S.F. Covalla, T.L. Woodard, and D.R. Lovely. Biofilm and nanowire production leads to increased current in Geobacter sulfurreducens fuel cells. *Appl. Environ. Microb.,* 2006 72(11): 7345-7348, doi:10.1128/AEM.01444-06.

11. Tender, L.M., C.E. Reimers, H.A. Stecher, D.E. Holmes, D.R. Bond, D.L. Lowry, K. Pilobello, S.J. Fertig, and D.R. Lovely. Buried treasure; harnessing microbial power generation on the seafloor. *Nat. Biotechnol.,* 2002 20: 821-825.

12. Whitfiled, M. The Electrochemical Characteristics of Natural Redox Cells. *Limnol Oceanogr.,* 1972 17(3):13 383-393.

13. Gorby, Y.A., Yanina S., McLean J.S., Rosso K.M., Moyles D., Dohnalkova A., Beveridge T.J., Chang I.S., Kim B.H., Kim K.S., Culley D.E., Reed S.B., Romine M.F., Saffarini D.A., Hill E.A., Shi L., Elias D.A., Kennedy D.W., Pinchuk G., Watanabe K., Ishii S., Logan B., Nealson K.H., Fredrickson J.K. Electrically conductive bacterial nanowires produced by Shewanella oneidensis strain MR-1 and other microorganisms. *Proc Natl Acad Sci USA,* 2006 103(30):11358–11363.

14. Kim, B.H., Kim H.J., Hyun M.S., Park D.H., Direct electrode reaction of Fe(III)-reducing bacterium, Shewanella putrefaciens. *J Microbiol Biotechnol,* 1999 9(2):127–131.

15. Kim, G.T., Hyun M.S., Chang I.S., Kim H.J., Park H.S., Kim B.H., Kim S.D., Wimpenny J.W., Weightman A.J. Dissimilatory Fe(III) reduction by an electrochemically active lactic acid bacterium phylogenetically related to Enterococcus gallinarum isolated from submerged soil. *J Appl Microbiol,* 2005 99(4):978–987.

16. Jung, S. and J.M. Reagan. Comparison of Anode Bacterial Communities and

Performance in Microbial Fuel Cells with Different Electron Donors. *Appl Microbiol Biotechnol*, 2007 77:393–402.

17. Chaudhuri, S.K., Lovley D.R. Electricity generation by direct oxidation of glucose in mediatorless microbial fuel cells. *Nat Biotechnol,* 2003 21(10):1229–1232.
18. Park, H.S., Kim B.H., Kim H.S., Kim H.J., Kim G.T., Kim M., Chang I.S., Park Y.K., Chang H.I. A novel electrochemically active and Fe (III)-reducing bacterium phylogenetically related to Clostridium butyricum isolated from a microbial fuel cell. *Anaerobe,* 2001 7(6):297–306.
19. Rabaey, K., Boon N., Siciliano S.D., Verhaege M., Verstraete W. Biofuel cells select for microbial consortia that self-mediate electron transfer. *Appl Environ Microbiol,* 200470(9):5373–5382.
20. Nielson, M.E., C.E. Reimers, H.A. Stecher III, Enhanced Power from Chambered Benthic Microbial Fuel Cells. *Environ Sci Technol.,* 2007 41(22): 7895-7900.
21. Reimers, C.E., L.M. Tender, S. Fertig, and W. Wang. Harvesting energy from the marine sediment-water interface. *Environ. Sci. Technol.,* 2001 35: 192-195.
22. Holmes, D.E., D.R. Bond, R.A O'Neil, C.E. Reimers, L.R. Tender, D.R. Lovley. Microbial Communities Associated with Electrode Harvesting Electricity from a Variety of Aquatic Sediments. *Microb Ecol,* 2004 4(48):178-190.
23. Pham, C.A., Jung S.J., Phung N.T., Lee J., Chang I.S., Kim B.H., Yi H., Chun J., A novel electrochemically active and Fe(III)-reducing bacterium phylogenetically related to Aeromonas hydrophila, isolated from a microbial fuel cell. FEMS *Microbiol Lett* 2003, 223(1):129–134.
24. Higuchi, R., C. Fockler, G. Dollinger, R. Watson. Kinetic PCR Analysis: Real-time Monitoring of DNA Amplification Reactions. *Nat Biotechnol, 1993.* 11:1026-1030.

25. Wong, M. L., and J. F. Medrano. Real-time PCR for mRNA quantitation. *Biotechniques* 2005 39: 75-85.

26. Bio-Rad Laboratories, Inc. Sub-Cell® GT Agarose Gel Electrophoresis Systems Instruction manual. *www.biorad.com* Published online 2008.

27. ERG Aerospace, Technical Data for Duocel® Graphite Foam, *http://www.ergaerospace.com/Descriptors.htm*, Published online 2011.

28. Koopers Inc. Technical data for Kfoam® graphite foam. *http://www.kfoam.com/mainsite/material.htm*, Published online 2009.

29. Zymo Research Corporation. Instruction Manual for the ZR Soil Microbial DNA Kit. Catalog Number D6001. *http://www.zymoresearch.com/content/protocols-zymo-research. 2007*

30. Suzuki, M.T., L.T. Taylor, and E.F. DeLong. Quantitative Analysis of Small-Subunit rRNA Genes in Mixed Microbial Population via 5'- Nuclease Assays. *Appl. Environ. Microbio.* 2000 66(11):4605-4614.

31. Stults, J.R., O. Snoeyenbos-West, B. Methe, D.R. Lovley, and D.P. Chandler. Application of the 5' Fluorogenic Exonuclease Assay (Taqman) for Quantitative Ribosomal DNA and rRNA Analysis in Sediments. *Appl. Environ. Microbio.,* 2001. 67(6): 2781-2789.

32. Beller, H.R., S.R. Kane, T.C. Legler, and P.J.J. Alverez. A Real-Time Polymerase Chain Reaction Method for Monitoring Anaerobic, Hydrocarbon-Degrading Bacteria Based on a Catabolic Gene. *Environ. Sci. Technol.,* 2002 36:3977-3984.

33. Livak, K. J., and T. D. Schmittgen. Analysis of Relative Gene Expression Data Using Real Time Quantitative PCR and the 2-ΔΔĆT Method. *Methods* 2001 25(4): 402-408.

34. Bio-Rad Laboratories, Inc. Real-Time PCR Applications Guide. *www.biorad.com* Published online 2006.

35. Muyzer, G. and K. Smalla. Application of Denaturing Gradient Gel Electrophoresis (DGGE) and Temperature Gradient Gel Electrophoresis (TGGE) in microbial ecology. A Van Leeuw *J Microb,* 1998 73: 121-141.

36. Liu, Hong, S. Cheng, B. Logan. Power Generation in Fed-Batch Microbial Fuel Cells as a Function of Ionic Strength, Temperature, and Reactor Configuration. *Environ Sci Technol 2005* 39(14): 5488-5493.

37. Mohan, S. V., S.V. Raghavulu, P.N. Sarma. Influence of Anodic Biofilm Growth on Bioelectricity Production in Single Chambered Mediatorless Microbial Fuel Cell Using Mixed anaerobic Consortia. *Biosens Bioelectron* 2008 24: 41-47.

38. Poco Graphite, Inc. Pocofoam® Technical Material Properties. *http://www.poco.com/Portals/0/Literature/Semiconductor/78962v2PocoFoamFlyer.pdf.* Published online 2008.

39. Maclean, D., J. D. G. Jones, and D. J. Studholme, Application of 'Next-Generation' Seqeuncing technologies to microbial genetics. *Nat Rev Microbiol* 2009. 7(4): 287-296.

40. Wotawa-Bergen, D.B., K.E. Richter, L.M. Tender, C.E. Reimers, Y. Gong, Operational Testing of Sediment Microbial Fuel Cells in San Diego Bay. *IEEE* 2010. ISBN 978-1-4244-4332-1.